Optical Performance of a Hybrid Compound Parabolic Concentrator and Parabolic Trough Concentrator System for Dual Concentration

Sridhar Sripadmanabhan Indira[1*], Chockalingam Aravind Vaithilingam[1*], Ramsundar Sivasubramanian[1] Kok-Keong Chong[2], R. Saidur [3,4], Kulasekharan Narasingamurthi[5]

[1] School of Engineering, Faculty of Innovation and Technology, Taylor's University Lakeside Campus, No. 1, Jalan Taylor's, 47500 Subang Jaya, Selangor, Malaysia.
[2] Lee Kong Chian Faculty of Engineering and Science, Universiti Tunku Abdul Rahman, Bandar Sungai Long, 43000 Kajang, Selangor, Malaysia.
[3] Research Centre for Nano-Materials and Energy Technology (RCNMET), School of Engineering and Technology, Sunway University, 47500 Subang Jaya, Malaysia.
[4] Department of Engineering, Lancaster University, Lancaster LA1 4YW, UK.
[5] Metier Technical Leader, Valeo India Private Limited, No. 63, Rajiv Gandhi Salai, Navallur, Chennai – 600130, India.

*Corresponding authors.

E-mail addresses: sridharsripadmanabhannadarindira@sd.taylors.edu.my, sibisri819@gmail.com (S. S Indira), chockalingamaravind.vaithilingam@taylors.edu.my, aravindcv@ieee.org (C.A. Vaithilingam).

Abstract

This work proposes a hybrid compound parabolic concentrator and parabolic trough concentrator (CPC/PTC) system for concentrator photovoltaic/thermal (CPV/T) and hybrid concentrator photovoltaic/thermal-thermoelectric generator (CPVT-TEG) applications. The geometrical design and optical analysis of the novel hybrid CPC/PTC system are discussed in the present study. Ray-tracing models were used to identify the different variables that influence the optical efficiency of both CPC and PTC. The concentration ratio (CR) of PTC in the hybrid CPC/PTC system is evaluated and compared with the standard PTC concentration ratio for various rim angles ranging from 15° to 75°. The results revealed that the loss in PTC concentration due to the CPC's shadow on the hybrid CPC/PTC system is reduced when the aperture width of the PTC is increased. The maximum optical efficiency of the hybrid CPC/PTC system for 0° incident angle is ~73% which is ~6.35% higher than standard PTC. Finally, the proposed hybrid CPC/PTC system's overall optical efficiency is evaluated under various tracking modes for equinox, summer solstice, and winter solstice. The results imply that the dual-axis tracking CPC/PTC system achieves a constant optical efficiency of ~70%.

Keywords:

Compound parabolic concentrator, parabolic trough concentrator, concentrator photovoltaics, Monte-Carlo ray-tracing, optical efficiency.

Nomenclature

C	Concentration ratio (suns)
C'_{PTC}	modified concentration ratio of PTC in hybrid CPC/PTC system
W	aperture width of the concentrator
W'	receiver width
L	length of CPC/PTC
L'	length of CPC/PTC receiver
f	focal length of the concentrator
h	height of the concentrator
$K_{CPC}(\phi_i)$	incident angle modifier of CPC
$K_{PTC}(\phi_i)$	incident angle modifier of PTC
l	curvilinear length of the PTC
I_{DIF}	diffuse solar radiation
I_t	incident total solar radiation
I_{ref}	solar radiation under standard test condition
A	area of the inlet aperture
A'	area of the receiver

Symbols

θ_c	full CPC's half-acceptance angle
θ_H	HEMR CPC's half-acceptance angle
θ_L	LEMR CPC's half-acceptance angle
θ_T	full CPC's truncation angle
θ_{TH}	HEMR CPC's truncation angle
θ_{TL}	LEMR CPC's truncation angle
τ_H	curve parameter of HEMR CPC
τ_H	curve parameter of LEMR CPC
φ_r	rim angle of PTC
α	half angular width of incident solar radiation (0.267°)
ρ_{PTC}	reflectivity of PTC
α_{CPC}	absorbance of the CPC receiver
α_{CPC}	absorbance of the PTC receiver

γ_{PTC}	intercept factor
ϕ_i	incident angle
$\zeta(\phi_i)$	geometrical end losses
τ_{CPC}	effective transmissivity of the CPC
ξ	correction factor for loss due to diffuse radiation in CPC
δ	declination angle
ω	solar hour angle
σ_I	standard deviation non-uniform factor

Subscripts

H	HEMR CPC
L	LEMR CPC
i	incidence
DIF	diffuse
DNI	direct normal irradiance
t	total
r	rim of PTC
Full	CPC without truncation

Abbreviations

CPC	Compound parabolic concentrator
PTC	Parabolic trough concentrator
CPV	Concentrator photovoltaics
LCPV	Low concentrator photovoltaics
CPVT	Concentrator photovoltaics thermal
CR	Concentration ratio
TEG	Thermoelectric generators
STEG	Solar thermoelectric generators (solar absorber + TEG)
LFR	Linear fresnel reflectors
CSP	Concentrator solar power
EMR	Eliminations of multiple reflections
BCP	Best concentration plane
N-S	North-South
E-W	East-West

1. Introduction

Solar energy is a propitious renewable energy source as it is a copious source of heat and electricity. Moreover, solar energy does not turn out any greenhouse gases and has the least negative effect on the environment than other energy sources. As per the world energy outlook 2020, solar power is the least expensive electricity source ever seen [1]. The use of active solar power was relatively slow until the 18th century. During this period, the English scientist Joseph Priestley and French chemist Lavoisier utilised large focusing lenses to concentrate the sun's energy for combustion. The discovery of the photovoltaic effect in 1839 by Becquerel paved the way for advancing solar energy harvesting technologies. Solar energy can be actively transformed into electricity using photovoltaic technology and solar thermoelectric generators. On the other hand, solar flat plate collectors and concentrators convert the sun's heat into useful energy at various temperature ranges. Later, hybrid CPV/T, CPV-TEG, and CPVT-TEG were developed to generate both electric and thermal energy. The hybrid combination of CPVT and TEG systems produced higher system efficiencies than individual PV and solar thermal technologies. Several research works have focused on the combination of solar PV/T with thermoelectric modules [2-5]. Concentrators like CPC, PTC, LFR, fresnel lens, parabolic dish, and v-trough are widely employed in CSP, CPV/T, CPV-TEG, CPVT-TEG hybrid systems [6].

The first CPV/T collector was developed in Sandia Laboratories using Fresnel lenses in 1976 [7]. The reflector/mirror-based PTCs and CPCs are widely used along with fresnel lens and Fresnel reflectors in CPV/T systems. Gibart [8] and Chenlo and Cid [9] explored the manufacturing process for Fresnel lens and PTC based linear CPV/T systems. Chemisana et al. [10, 11] designed a CPV/T system for building integration applications by combining a domed linear fresnel lens and a compound parabolic concentrator. The system achieved a maximum concentration ratio of 10x. Furthermore, ray-tracing was used to improve the optical accuracy, thermal and electrical design, and building integrability. Several studies on parabolic trough and Fresnel based CPV/T setups were reviewed by Kasaeian et al. [12]. Nilsson et al. [13] developed an asymmetric compound parabola based CPV/T and evaluated its long term annual performance. Later, Chaabane et al. [14] constructed and analysed a linear CPVT setup using an unsymmetric compound parabolic concentrator. The CPVT system's maximum obtained thermal and electrical efficiency was equal to 16% and 10%. The PTC was used for the CPV/T system by Coventry et al. [15] in their study. The performance of the system was found to be 69%. Yongfeng et al. [16] developed a PTC based CPV whose optical efficiency is 69%. Similar CPV/T studies were also performed using PTCs [17][18][19].

Ali et al. [20] established a new configuration of static three-dimensional elliptical hyperboloid concentrator (3-D EHC) and evaluated its optical performance. The concentration ratio of the 3-D EHC is 20x, and the optical efficiency is found to be 27%. Sellami et al. [21], in their research, calculated the optical efficiency and optical flux distribution of a static 3-D crossed compound parabolic concentrator (CCPC) for various solar incident angles. The CCPC's overall optical efficiency was discovered to be 95%, but the optical flux distribution analysis using 3-D ray tracing revealed that the flux distribution at the receiver was not uniform. Li et al. [22] proposed a novel static integrated CPC made up of a mirror CPC and a lens wall structure. The optical performance of the novel CPC was determined using the ray-tracing technique at various incidence/transverse angles. The optical efficiency of the CPC ranges between 56% - 70%. Kamnapure et al. [23], in their optical analysis of PTC with flat CPV receiver, analysed the impact of geometrical concentration ratio, slope error, and tracking error on the optical performance. The optical performance was analysed from the intercept factor calculation, for which an optical simulation tool called Advanced System Analysis Program (ASAP) is used.

Abdullahi et al. [24] investigated the possibility of using two tubular receivers and elliptical receivers in compound parabolic concentrators. The ray-tracing results showed that the horizontally aligned two tubular receiver and elliptical receiver CPCs outperforms the single receiver and vertically aligned receiver CPCs. Rehman et al. [25] put forth a novel design for PTC based solar collector for the thermoelectric power generator. The study investigates the effect of vertex angle and focus offset on the optical performance using the ray-tracing technique. The collector showed maximum optical performance of 93.61% when the vertex and focus offset were 130° and 20 mm, respectively. Khalid et al. [26] investigated the optical performance of two types of CPCs called lower-position-truncated CPC (LEMR) and higher-position-truncated CPC (HEMR), which has the absorber at the best concentration plane (BCP). The LEMR and HEMR CPCs can receive uniform solar flux at BCP compared with standard CPC with the flat absorber. This type of CPCs is used for LCPV/T applications.

Various hybrid PV/TEG, CPV/TEG, and CPV/T-TEG configurations have been studied in the literature (Fig. 1.). According to the literature survey, the majority of hybrid CPV-TEG and CPV/T-TEG systems use either a PTC or a Fresnel lens for concentration. Although PTC and Fresnel lenses can produce high solar concentration ratios, the flux received is not uniform. Due to non-uniform flux distribution, hybrid systems that use Fresnel lenses and PTC to focus sunlight on PV cells can cause hotspots, affecting the PV cells in the long

run. In existing Fresnel and PTC-based hybrid CPV-TEG configurations, multijunction solar cells and TEGs can produce more stable power output than crystalline silicon, amorphous silicon and polymer solar cells [27, 28]. TEGs are typically integrated on the rear side of the PV cells in the hybrid PV-TEG and CPV-TEG systems to harness excess heat from PV and generate electricity based on the temperature gradient between the hot and cold junctions of the TEG. In their study with TEGs integrated on the rear side of PV, Bjork and Nielsen [29] discovered that the drop in PV performance due to excess heat is higher than the power generated by TEG due to TEG's lower efficiency.

In 2019 Abdo et al. [30] came up with a novel type of CPV-STEG in which the TEG module was not directly integrated on the rear side of PV; instead, the TEG was directly focused with concentrated light. They had used two separate linear Fresnel lenses and reflectors to concentrate both the PV and TEG. In addition, for efficient cooling, a micro-channel heat sink was used in between the PV and TEG. In Abdo et al. [30], the optical analysis to study the flux distribution on both the PV and TEG is not done; instead, uniform solar radiation on PV and TEG is assumed to simplify the simulation. Furthermore, with PTC and Fresnel lens-based concentrator systems, we can use only multi-junction solar cells, but these solar cells are more expensive than silicon solar cells. Therefore, in this study, a hybrid solar concentrator system is introduced that can use less expensive silicon solar cells while also overcoming non-uniform flux distribution on the solar cells.

The present study proposes a hybrid CPV/T-TEG concentrator system with a low concentrating EMR CPC to direct solar radiation on PV cells and a high concentrating PTC to direct solar radiation on TEG, with a mutual cooling channel between PV and TEG to harness thermal energy. The EMR CPC employs less expensive silicon solar cells and can generate uniform solar flux on PV cells, thereby reducing hotspot heating. Furthermore, compared to Fresnel lens-based concentrator systems, the proposed hybrid CPC/PTC-based concentrator system can be easily retrofitted with existing PTC-based solar power plants.

As far as we know, there have been no CPV/T or CPV/T-TEG studies in which CPC has been combined with PTC; thus, the novelty of the current study is to design a hybrid CPC/PTC system with a flat receiver and evaluate its optical performance. In this study, a hybrid CPC/PTC system is optically analysed and compared for various rim angles and aperture widths using the Monte Carlo ray-tracing simulation method, which is simulated using commercial TracePro software [31]. TracePro is an optomechanical software used in optical

designing and flux uniformity studies of solar concentrators [32,33]. The effect of concentration ratio on irradiance distribution, non-uniformity, and optical efficiency of CPCs is also investigated in the present study. Furthermore, the effect of CPC on the optical performance of the PTC in a hybrid CPC/PTC for different rim angles and aperture widths is evaluated and compared to conventional PTC. Finally, the optical performance of the hybrid CPC/PTC in various tracking modes is compared and analysed. As a result, the current work is a proof-of-concept study on the feasibility of combining CPC and PTC to form a hybrid CPC/PTC solar concentrator for CPV/T and CPVT-TEG applications.

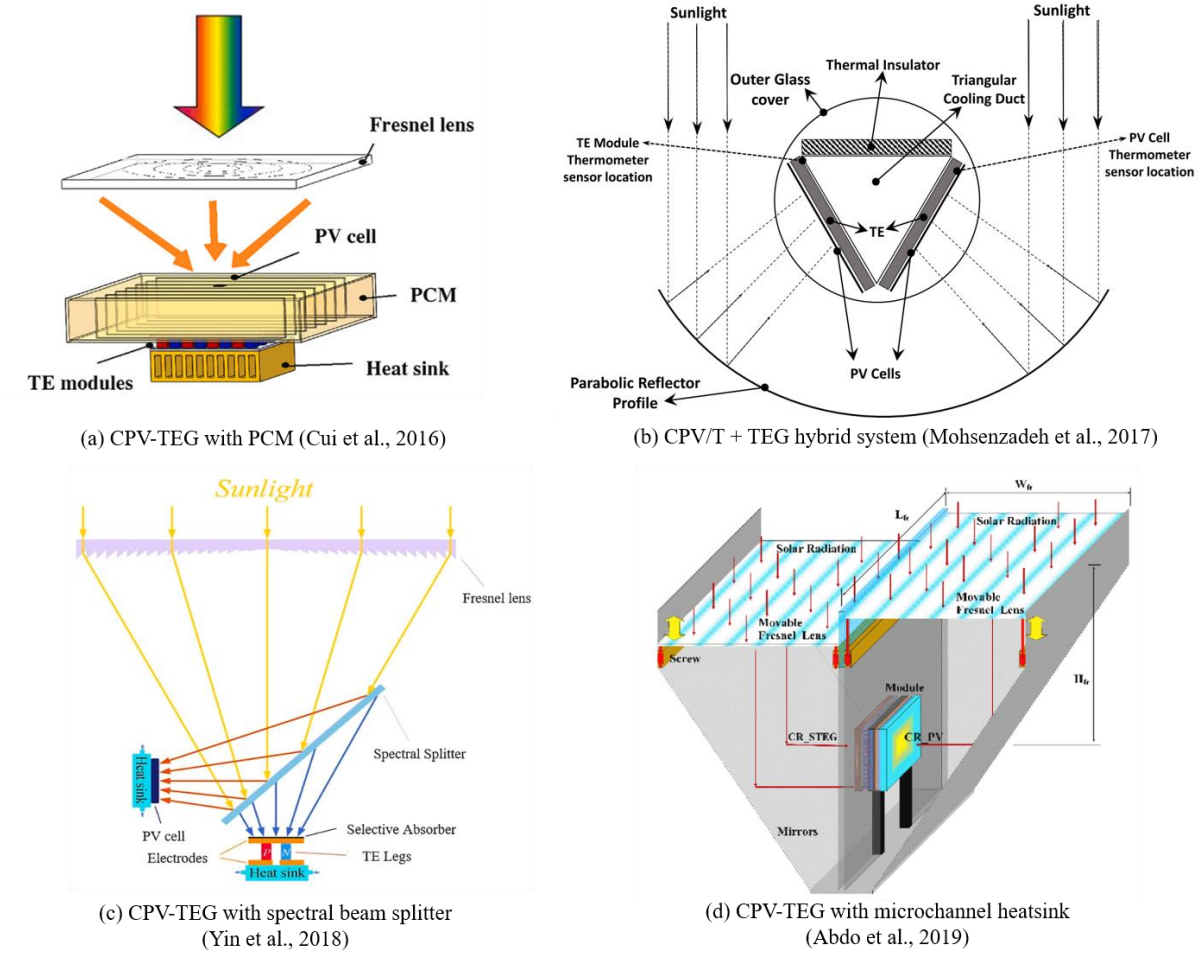

(a) CPV-TEG with PCM (Cui et al., 2016)

(b) CPV/T + TEG hybrid system (Mohsenzadeh et al., 2017)

(c) CPV-TEG with spectral beam splitter (Yin et al., 2018)

(d) CPV-TEG with microchannel heatsink (Abdo et al., 2019)

Fig. 1. Various types of solar concentrators used in hybrid CPVT-TEG system

2. Proposed Design

The schematic of the hybrid CPC/PTC system established in this work is shown in Fig. 2(a), and the 3D model is shown in Fig. 2(b). As shown in Fig. 2, the proposed structure consists of a 2D-CPC combined with linear PTC sharing a mutual rectangular cooling channel between the 2D-CPC and PTC receiver. The bottom PTC is optimised to take into account the shading effect of the top CPC. CPC is preferred because it can collect both beam and diffuse

solar radiation. The thermal efficiency of the stationary CPC decreases as incident solar radiation increases. According to studies, tracking CPC can collect 75% more energy than identical fixed CPC [34]. The thermal efficiency of a tracking CPC is more stable and 14.9 % higher than that of a stationary CPC [35]. As a result, the proposed hybrid CPC/PTC design with an integrated solar tracking mechanism is recommended.

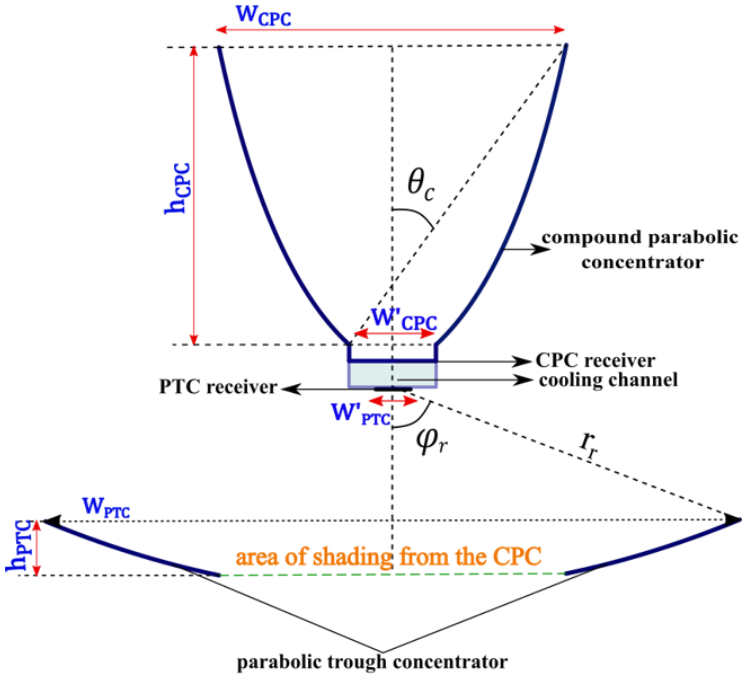

(a) Schematic of the proposed hybrid CPC/PTC system

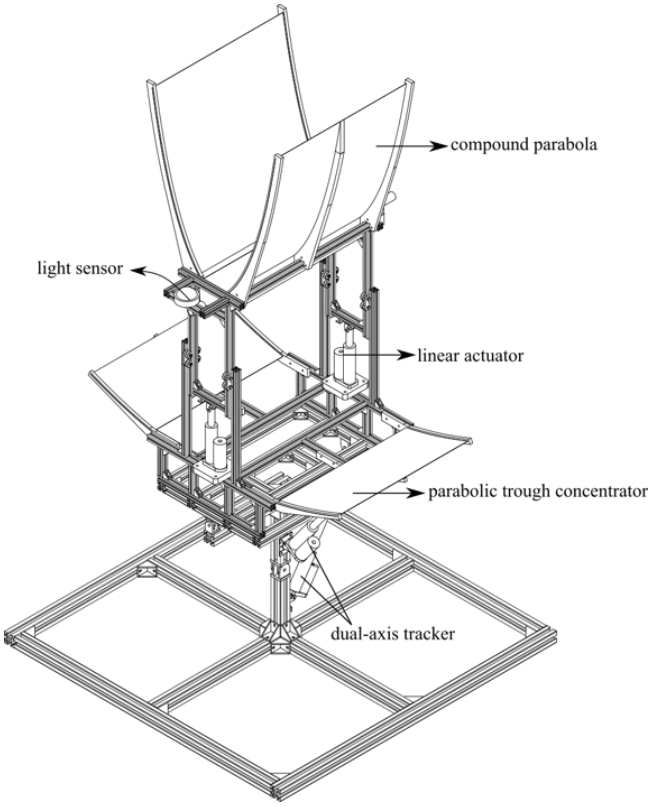

(b) 3D model of the proposed hybrid CPC/PTC prototype

Fig. 2. Description of the proposed hybrid CPC/PTC system

3. Methodology

As shown in Fig. 3, the optical performance of the proposed hybrid CPC/PTC structure is investigated in three parts. To design the hybrid CPC/PTC system, the analytical equations of the CPC and PTC geometries are first worked out. The second part employs TracePro software to run a Monte-Carlo ray-tracing simulation to investigate the various parameters influencing the optical performance of the hybrid CPC/PTC system. Finally, the optical efficiency of the hybrid CPC/PTC system under different tracking modes is investigated using the TracePro software's Solar Emulator tool.

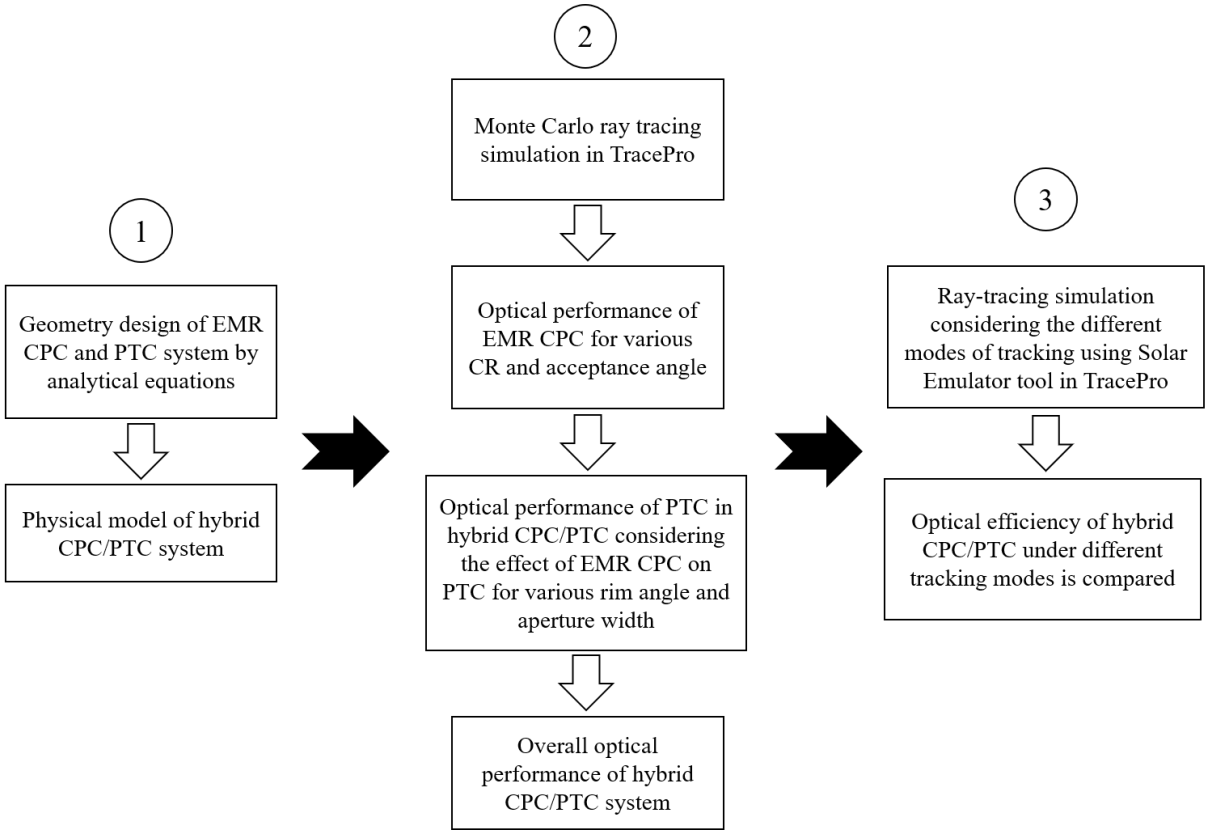

Fig. 3. Flowchart of the whole procedure for investigating the optical performance

3.1 Geometry modelling of 2D-CPC

The CPC is a non-imaging solar concentrator with two parabolic concentrators on its sides, as shown in Fig.2. The half acceptance angle θ_c is the angle formed by the axis of CPC and the line connecting the focus of one side parabola to the opposite edge of the aperture. The concentration ratio of a CPC (C_{CPC}) is a function of the half acceptance angle θ_c. For a two-dimensional CPC, the relation between C_{CPC} and θ_c is given as [36,37],

$$C_{CPC} = \frac{1}{sin\theta_c} = \frac{W_{CPC}}{W'_{CPC}} \quad (1)$$

The concentration ratio is also defined as the ratio of CPC's inlet and outlet aperture widths. There is no standard procedure for determining the acceptance half-angle value because it is calculated based on the concentration ratio that corresponds to the application for which the CPC collector is used. The inlet aperture and focus of CPC are also related to θ_c which is given as,

$$f_{CPC} = \frac{W'_{CPC}}{2}(1 + sin\theta_c) \quad (2)$$

where W'_{CPC} is the width of the CPC receiver and f_{CPC} is the focal length of CPC. The full height of the CPC is given by,

$$h_{CPC} = \frac{f_{CPC} cos\theta_c}{sin^2\theta_c} \tag{3}$$

In a full CPC at the parabola's upper-end points, the surfaces are almost parallel to the CPC's symmetry plane, thus contributing very little in concentrating radiation to the receiver. Hence, the full CPC can be truncated to a certain height to conserve the reflector area while retaining a reasonable level of performance.

The principle of eliminating multiple reflections (EMRs) is used in the current study for CPC truncation to produce uniform irradiance distribution on the CPC receiver [38, 39]. In general, the distribution of solar radiation received on the CPC's outlet aperture will be extremely non-homogeneous. However, in EMR CPC, the outlet aperture will be at a lower position (see Fig. 4), which is called as best concentration plane (BCP) [26]. As shown in Fig. 4, using the EMR principle, the CPC can be truncated in two possible ways: truncation at the highest position and truncation at the lowest position. The acceptance angle, focal length and height of both HEMR and LEMR are given by the following equations [39]:

$$\begin{aligned}
&16(sin^2\theta_H + sin\theta_H)\tau_H^4 + 8(3sin^2\theta_H + sin\theta_H - 1)\tau_H^2 + (-16sin\theta_H cos\theta_H)\tau_H \\
&\qquad + (-3sin^2\theta_H + sin\theta_H + 2) = 0 \\
&4\overline{B_H B'_H}(sin\theta_H cos\theta_H + cos\theta_H)\tau_H^2 + 4\overline{B_H B'_H}(sin^2\theta_H + sin\theta_H)\tau_H \\
&\qquad - (\overline{B_H B'_H} sin\theta_H cos\theta_H + \overline{B_H B'_H} cos\theta_H + 2h_{HEMR\,CPC} = 0 \\
&4(sin^2\theta_H + sin\theta_H)\tau_H^2 - 4(sin\theta_H cos\theta_H + cos\theta_H)\tau_H \\
&\qquad - (sin^2\theta_H + sin\theta_H - C_{HEMR\,CPC} - 1) = 0 \\
&\overline{B_H B'_H}(sin\theta_H + 1) - 2f_H = 0
\end{aligned} \tag{4}$$

$$\begin{aligned}
&16(sin^2\theta_L + sin\theta_L)\tau_L^4 + (32sin^2\theta_L + 8sin\theta_L - 4)\tau_L^2 \\
&\qquad + 8sin\theta_L cos\theta_L(tan^2\theta_L - 2)\tau_L + (-5sin^2\theta_L + sin\theta_L + 1) = 0 \\
&4\overline{B_L B'_L}(sin\theta_L cos\theta_L + cos\theta_L)\tau_L^2 + 4\overline{B_L B'_L}(sin^2\theta_L + sin\theta_L)\tau_L \\
&\qquad - \left(\overline{B_L B'_L} sin\theta_L cos\theta_L + \overline{B_L B'_L} cos\theta_L + 2h_{LEMR\,CPC}\right) = 0 \\
&4(sin^2\theta_L + sin\theta_L)\tau_L^2 - 4(sin\theta_L cos\theta_L + cos\theta_L)\tau_L \\
&\qquad - (sin^2\theta_L + sin\theta_L - C_{LEMR\,CPC} - 1) = 0 \\
&\overline{B_L B'_L}(sin\theta_L + 1) - 2f_L = 0
\end{aligned} \tag{5}$$

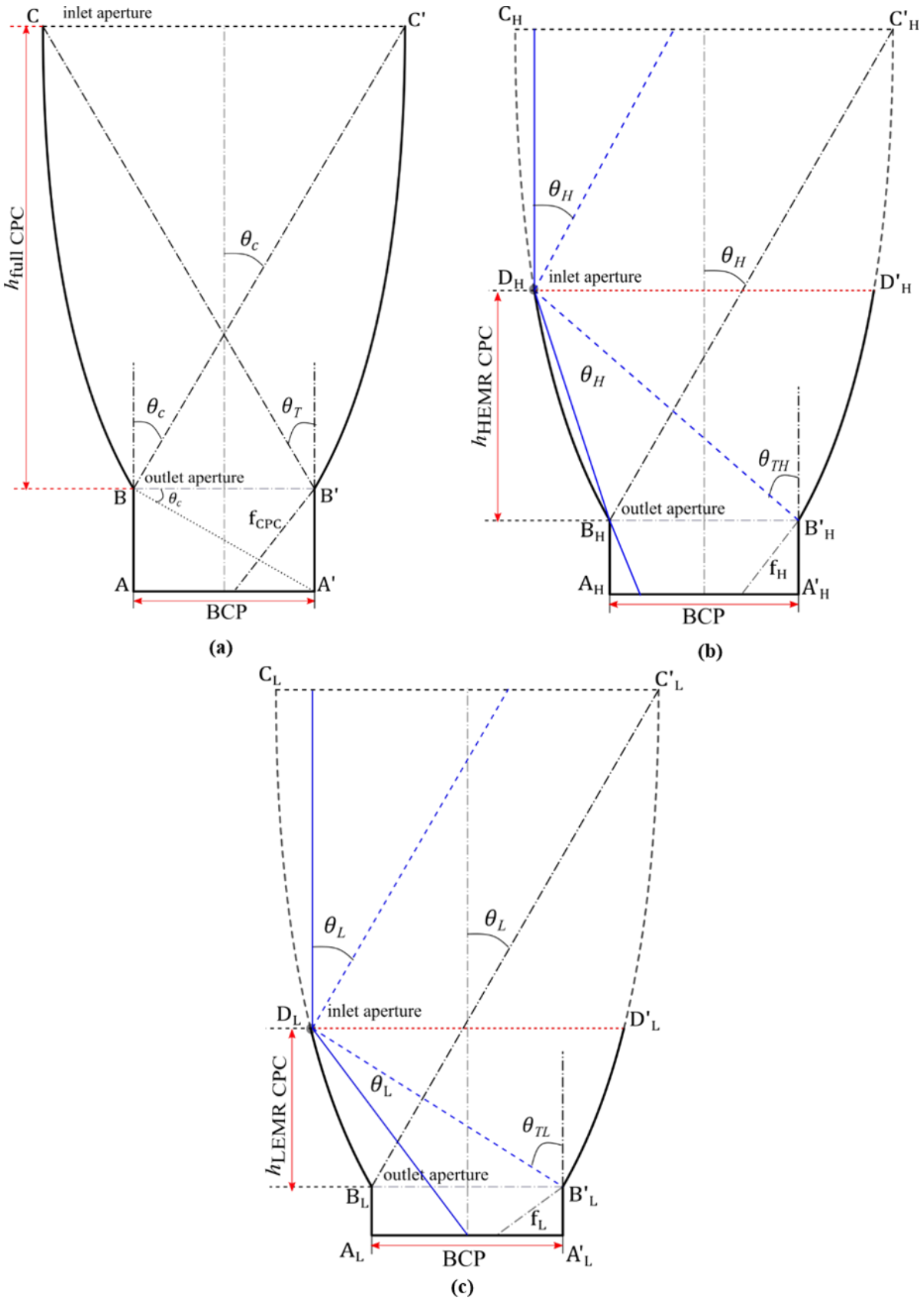

Fig. 4. Schematic of (a) Full CPC, (b) HEMR CPC (c) LEMR CPC

As stated earlier, the irradiance distribution at any CPC's outlet aperture would be non-uniform. As a result, solar irradiance will be obtained at a lower position, known as the BCP. Eq. (6) can be used to determine the distance across the outlet aperture and the BCP.

$$BA = \frac{\overline{BB'}}{tan\theta_c} \qquad B_H A_H = \frac{\overline{B_H B'_H}}{tan\theta_H} \qquad B_L A_L = \frac{\overline{B_L B'_L}}{tan\theta_L} \tag{6}$$

The design parameters of HEMR and LEMR CPCs are calculated using equations (1) – (6) and are listed in Table 1.

Table 1. Design parameters of Full, HEMR, and LEMR CPCs with receiver width 125 mm

C_{CPC}	Type of CPC	Half-acceptance angle (°)	Width of aperture (mm)	Height of CPC (mm)	Focal length (mm)	Truncation Angle (°)	Height of flat reflectors (mm)
2	Full	30	250	324.8	93.75	30	72.168
	HEMR	26.49	249.99	188.7	90.38	26.49	62.295
	LEMR	19.4	249.98	133.5	83.26	19.4	44.019
3	Full	19.47	375.0225	707.1	83.33	19.47	44.191
	HEMR	15.6	375	361.2	79.31	15.6	34.9
	LEMR	10.18	374.96	267.2	73.54	10.18	22.446
4	Full	14.48	499.92	1210	78.12	14.48	32.28
	HEMR	10.61	499.98	563.5	74	10.61	23.415
	LEMR	6.607	499.99	435.4	69.69	6.607	14.478
5	Full	11.54	625	1837	75	11.54	25.522
	HEMR	7.782	625.01	797.1	70.96	7.782	17.082
	LEMR	4.719	624.98	636.3	67.64	4.719	10.3186
6	Full	9.594	750	2588	72.92	9.594	21.1287
	HEMR	5.992	749.96	1062	69.02	5.992	13.120
	LEMR	3.566	749.98	869.3	66.39	3.566	7.7898
7	Full	8.213	875.022	3464	71.43	8.213	18.0417
	HEMR	4.774	875.067	1359	67.7	4.774	10.4394
	LEMR	2.8	874.958	1134	65.55	2.8	6.1135
8	Full	7.181	1000	4465	70.31	7.181	15.749
	HEMR	3.902	1000.06	1687	66.75	3.902	8.526
	LEMR	2.261	998.72	1430	64.97	2.261	4.9352

3.2 Geometry modelling of PTC

The linear PTC is an imaging type concentrator used for applications requiring a temperature range of 100 to 500 °C. The PTC with a flat absorber and various essential factors is shown in Fig. 2(a). The rim angle (φ_r), aperture width (W_{PTC}), receiver width (W'_{PTC}), focal length (f_{PTC}), height (h_{PTC}), and the concentration ratio (C_{PTC}) are the factors that must be considered when modelling parabolic troughs geometrically. The following expression gives the parabolic shape profile in terms of a coordinate system,

$$y = \frac{x^2}{4f_{PTC}} \tag{7}$$

The radius (r) and rim radius (r_r) of the parabolic reflector is given as [36],

$$r = \frac{2f_{PTC}}{1 + cos\varphi} \tag{8}$$

$$r_r = \frac{2f_{PTC}}{1 + cos\varphi_r} = \frac{W_{PTC}}{2sin\varphi_r} \tag{9}$$

The rim angle (φ_r) can be derived from the aperture width, focal distance, and rim radius (r_r) [36]

$$\varphi_r = tan^{-1}\left[\frac{8\frac{f_{PTC}}{W_{PTC}}}{16\left(\frac{f_{PTC}}{W_{PTC}}\right)^2 - 1}\right] = sin^{-1}\left(\frac{W_{PTC}}{2r_r}\right) \tag{10}$$

The height of PTC depends on the aperture width and focal length, as shown in the following equation [36],

$$h_{PTC} = \frac{W_{PTC}^2}{16f_{PTC}} \tag{11}$$

The width of the image formed on the flat receiver (W'_{PTC}) can be calculated from the aperture width and the rim angle [36],

$$W'_{PTC} = \frac{W_{PTC}sin\alpha}{\cos(\varphi_r + \alpha)} \tag{12}$$

The geometrical concentration ratio is defined as the PTC aperture area to the receiver area [36]:

$$C_{PTC} = \frac{W_{PTC}L_{PTC}}{W'_{PTC}L'_{PTC}} = \frac{W_{PTC}}{W'_{PTC}} \tag{13}$$

This geometrical concentration ratio of the PTC can be modified by considering the shading of the CPC,

$$C'_{PTC} = \frac{W_{PTC} - W_{CPC}}{W'_{PTC}} \tag{14}$$

The maximum possible concentration ratio that a PTC can obtain with a flat receiver is given as [40, 41]

$$C_{max,PTC} = \frac{1}{2sin\alpha} \cong 107 \tag{15}$$

where α is the half-acceptance angle, and the maximum it could be is 0.27° for an imaging type concentrator. The curvilinear length of the parabola is determined by the following formula [42],

$$l_{PTC} = 2f_{PTC}\left(w\sqrt{1+w^2} + \frac{1}{2}\ln\frac{\sqrt{1+w^2}+w}{\sqrt{1+w^2}-w}\right) \tag{16}$$

$$w = \frac{W_{PTC}}{4f_{PTC}} \tag{17}$$

3.3 Optical Modelling

3.3.1 Optical efficiency of CPC

Optical efficiency is the crucial parameter to determine in the optical modelling of a concentrator. The optical efficiency of CPC is the ratio of total solar radiation concentrated at the outlet aperture or BCP to the total solar radiation received at the inlet aperture of the CPC. The peak optical efficiency of CPC is given as [37]

$$\eta_{CPC} = \tau_{CPC} * \alpha_{CPC} * K_{CPC}(\phi_i) * \xi \tag{18}$$

In this equation τ_{CPC} is the effective transmissivity of the CPC, which account for specular reflectance and mean number of reflections. α_{CPC} is the absorptivity of the CPC receiver, $K_{CPC}(\phi_i)$ is the incidence angle modifier and ξ is the correction factor for the loss of diffuse irradiance beyond the acceptance angle. The factor ξ is determined by Eq. (19) [37]

$$\xi = 1 - \left(1 - \frac{1}{C_{CPC}}\right)\frac{I_{DIF}}{I_t} \tag{19}$$

where I_{DIF} is the diffuse solar radiation, and I_t is the total solar radiation.

3.3.2 Optical efficiency of PTC

The solar energy received by the PTC receiver strongly depends on its optical properties. The following equation gives the optical efficiency of the parabolic trough concentrator [43]

$$\eta_{PTC} = \rho_{PTC} * \alpha_{PTC} * \gamma_{PTC} * K_{PTC}(\phi_i) * \zeta(\phi_i) \tag{20}$$

In this equation ρ_{PTC} is the reflectance of the PTC, α_{PTC} is the absorptivity of PTC receiver, γ_{PTC} is the intercept factor, $K_{PTC}(\phi_i)$ is the incidence angle modifier, and $\zeta(\phi_i)$ is the geometrical end loss factor. The end loss factor accounts for the portion of the receiver length, which doesn't receive the concentrated solar rays from the PTC. The following equation estimates the end effect,

$$\zeta(\phi_i) = 1 - \left\{\left(\frac{f_{PTC}}{L_{PTC}}\right) * \left[1 + \left(\frac{W_{PTC}^2}{48 f_{PTC}^2}\right)\right] * tan\phi_i\right\} \quad (21)$$

The intercept factor (γ) of the PTC is defined as the ratio (0 to 1) of rays incident on the parabola aperture that reaches its receiver [44].

3.3.3 Optical efficiency of hybrid CPC/PTC system

The overall optical efficiency of the hybrid CPC/PTC is the ratio of solar radiation received at both CPC (Q'_{CPC}) and PTC (Q'_{PTC}) receiver to the solar radiation received at the inlet aperture of the CPC/PTC ($Q_{CPC/PTC}$) system, namely,

$$\eta_{CPC/PTC} = \frac{Q'_{CPC} + Q'_{PTC}}{Q_{CPC/PTC}} \quad (22)$$

$$Q'_{CPC} = C_{CPC} I_t \eta_{CPC} A'_{CPC} \quad (23)$$

$$Q'_{PTC} = C'_{PTC} I_{DNI} \eta_{PTC} A'_{PTC} \quad (24)$$

$$Q_{CPC/PTC} = I_t A_{CPC/PTC} \quad (25)$$

where A'_{CPC} is the area of the CPC receiver, A'_{PTC} is the area of the PTC receiver and I_{DNI} is the direct normal solar radiation.

3.4 Ray-tracing simulation

The Monte-Carlo ray-tracing simulation is an effective technique for modelling and optimising solar concentrator parameters like concentration ratio, intercept factor, and optical efficiency [45]. For optical modelling in this study, we used the TracePro ray-tracing software. Fig. 5 depicts the step-by-step process of ray-tracing simulation. We varied the CPC and PTC geometry for different concentration ratios in the analysis, and its performance was investigated. Solidworks was used to create the 3-D model of the concentrators and receiver, which was then imported into TracePro for ray-tracing analysis. The following are the assumptions for the ray-tracing simulation:

- Under surface properties, the reflecting part of the concentrator was defined as reflectors (commercially available MIRO 1 Alanod solar reflector is considered) whose reflectivity is 95%, and specular reflectance is approximately equal to 92% [17]. Two separate receivers were considered, and their surface absorptivity is set to 100 %.
- For ray simulation, two sources were established over the inlet aperture of the compound parabolic concentrator, as shown in Fig. 6. One source is considered direct normal irradiance (DNI 1 in Fig. 6), and the second source is considered diffuse

irradiance (hemispherical source DIF in Fig. 6). One direct normal irradiance source (DNI 2 in Fig. 6) is defined over its aperture for the parabolic trough concentrator. The grid pattern was set as random with 8 million uniformly distributed rays. For optical analysis, the DNI sources are defined over the inlet aperture of the concentrators with incident rays aligned to the concentrator axis. The number of rays' sensitivity is analysed using the irradiance profile of 2 HEMR CPC as an illustration (see Fig. 7).

- The average radiation intensity is considered as 984 W/m^{2,} and the spatial profile was defined as solar. The DNI source irradiance is set as 750 W/m^2, and the diffuse source irradiance is set as 234 W/m^2 [46]. All the incident solar rays are assumed with a half angle of 0.27°.
- The slope error due to surface and shape defects in imperfect concentrators are automatically quantified in TracePro simulation using the Bidirectional Scattering Distribution Function (BSDF) [17, 47]. The sun shape and circumsolar radiation effects are neglected as they are not significant as slope error [44]. The other error, like receiver location errors and misalignment errors, were neglected [31].

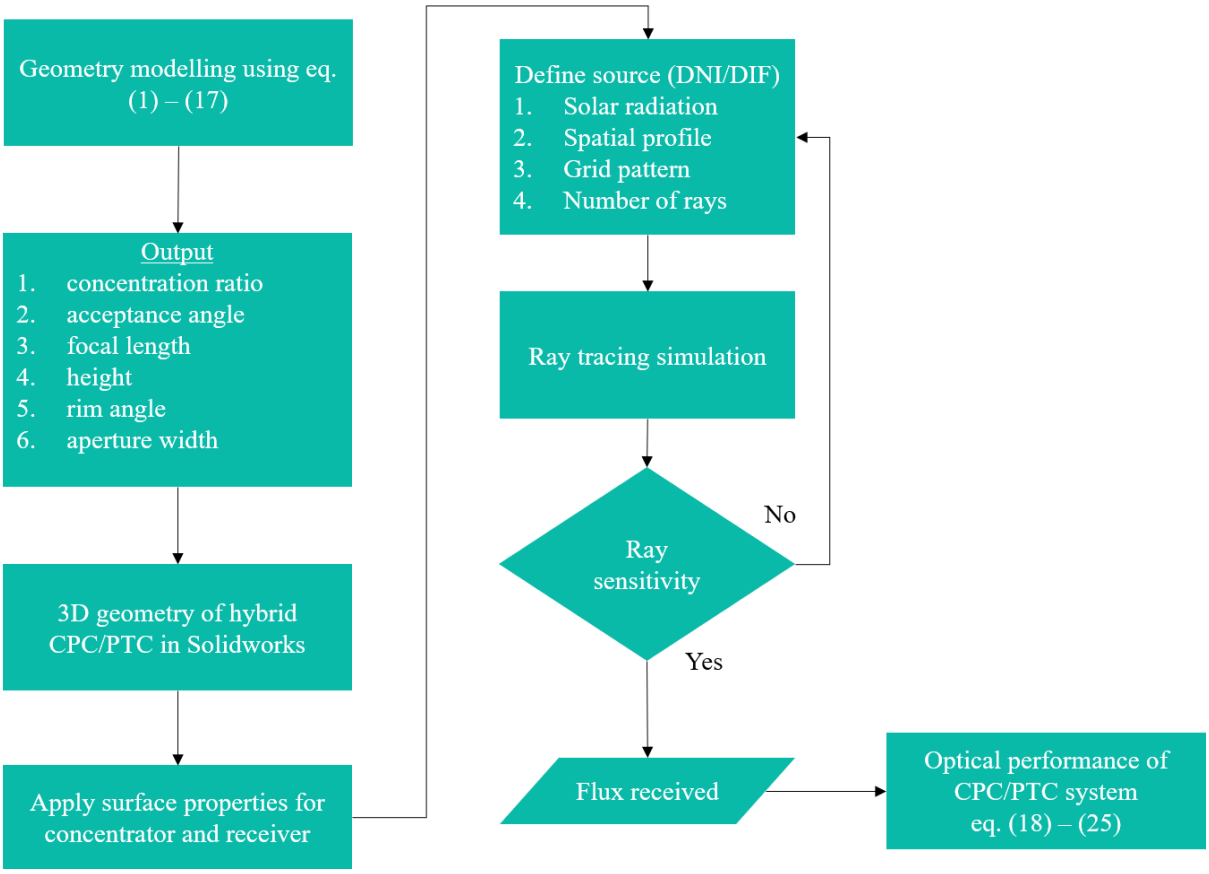

Fig. 5. Ray trace schema chart for hybrid CPC/PTC system

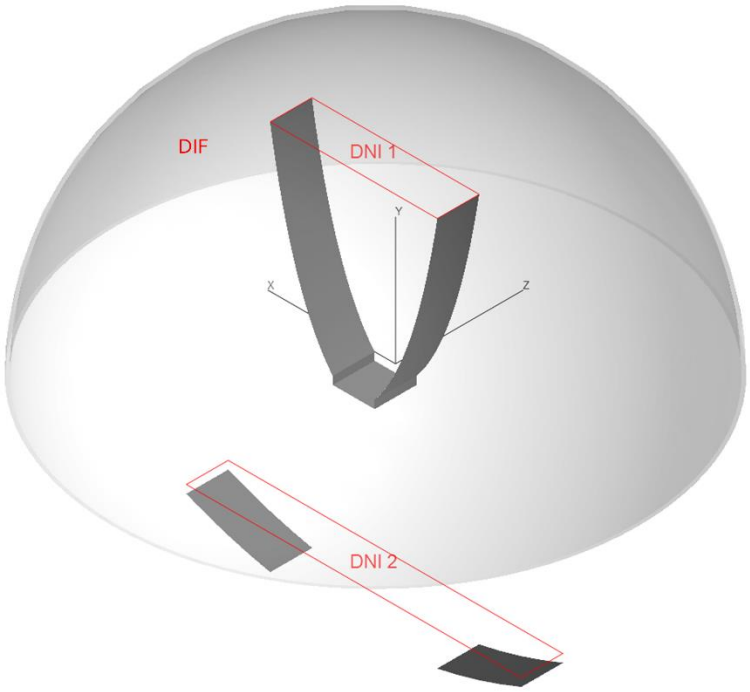

Fig. 6. Schematic of ray tracing simulation with DNI and DIF source in TracePro

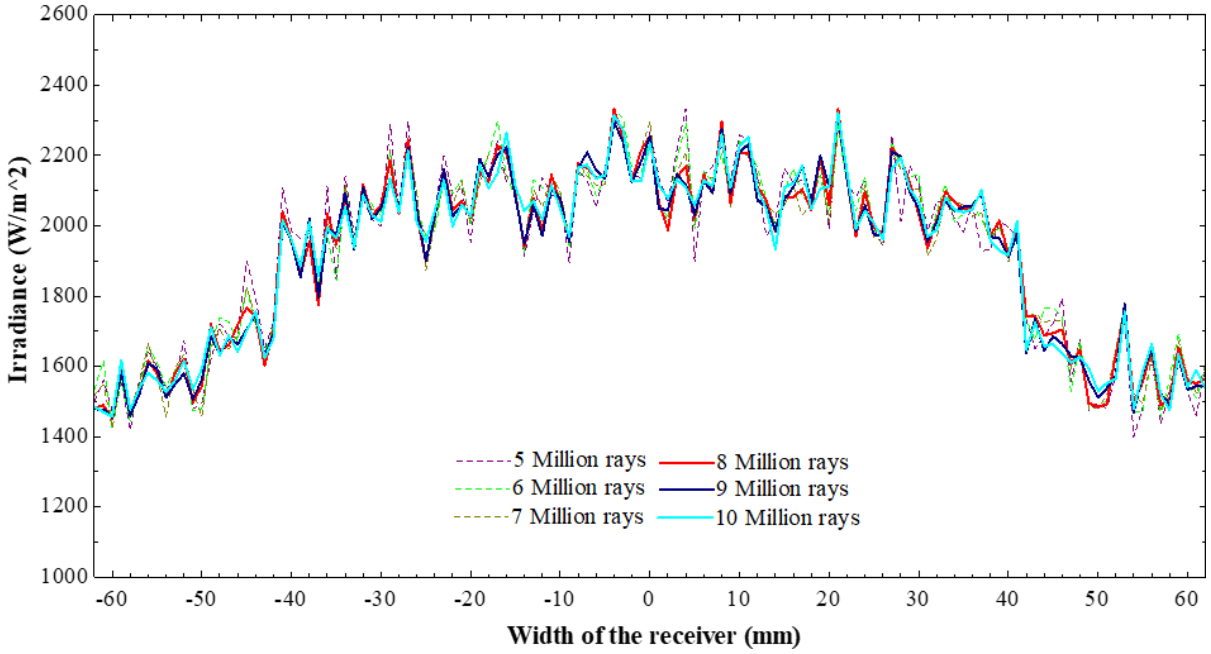

Fig. 7. Analysis of the number of rays' sensitivity

4. Optical efficiency of CPC/PTC under different modes of tracking

In the case of solar concentrators tracking mechanism is essential, which allows the concentrators to follow the sun for higher optical efficiency. The tracking can be classified based on their mode of operation as single-axis and dual-axis tracking. There are various ways of motion in single-axis tracking modes like east-west tracking on a polar north-south axis,

north-south tracking on a horizontal east-west axis, and east-west tracking on a horizontal north-south axis.

4.1 Dual-axis tracking:

In the dual-axis tracking mode, the concentrator and the receiver are continuously kept oriented towards the sun. The dual-axis tracking setup receives the maximum possible solar radiation, depending on the tracking mechanism's precision. Throughout the day, the angle of incidence on the concentrator will be kept at 0°, which can be mentioned as [37],

$$\cos \phi_i = 1 \tag{26}$$

4.2 East-west tracking on a polar north-south axis:

In this tracking mode, the concentrator's rotational axis is aligned along the north-south direction, and it follows the sun from east to west. The concentrator rotational axis is inclined at an angle that is similar to the geographical latitude. In this mode of tracking, the sun will be normal to the concentrator at equinoxes. The incidence angle is given as,

$$\cos \phi_i = \cos \delta \tag{27}$$

4.3 North-south tracking on a horizontal east-west axis:

The concentrator's axis of rotation will be aligned horizontally without any tilt in the east-west direction and traces the sun from north to south. The incidence angle in this mode of tracking is given as,

$$\cos \phi_i = \sqrt{1 - cos^2(\delta) sin^2(\omega)} \tag{28}$$

4.4 East-west tracking on a horizontal north-south axis:

The concentrator's rotational axis will be aligned horizontally without any tilt along the north-south direction and tracks the sun from east to west. The incidence angle is given as,

$$\cos \phi_i = \sqrt{sin^2(\alpha) + cos^2(\delta) sin^2(\omega)} \tag{29}$$

In the present study, the optical performance of the hybrid CPC/PTC system in various modes of tracking for the summer solstice, winter solstice and the equinoxes for the geographical location 3.0626° N 101.6168 °E (Jalan Taylor's, Malaysia). For this analysis, a 2

m long hybrid CPC/PTC system consisting of CR 4 HEMR CPC with 125 mm receiver width and PTC with 45° rim angle, 2 m aperture width, and 18.73 mm receiver width is considered. The solar radiation received by the hybrid CPC/PTC system under various tracking modes is simulated using the solar emulator tool in TracePro software [48]. The workflow of solar tracking using the Solar Emulator tool in TracePro software is illustrated in Fig. 8. The solar emulator tool calculates the sun's path based on the location's geographical latitude and longitude values. The ray simulation has been performed considering Igawa all-sky model under clear sky conditions. The type of model and sky condition considered here is not a concern, as it is used solely for comparison purposes. The hybrid system's position and tracking mode are configured using the Solar Emulator tool system setup and sun-tracking options. The graphical user interface of the Solar Emulator tool showing the location, source and system setup is illustrated in Fig. 23 (See Annexure B).

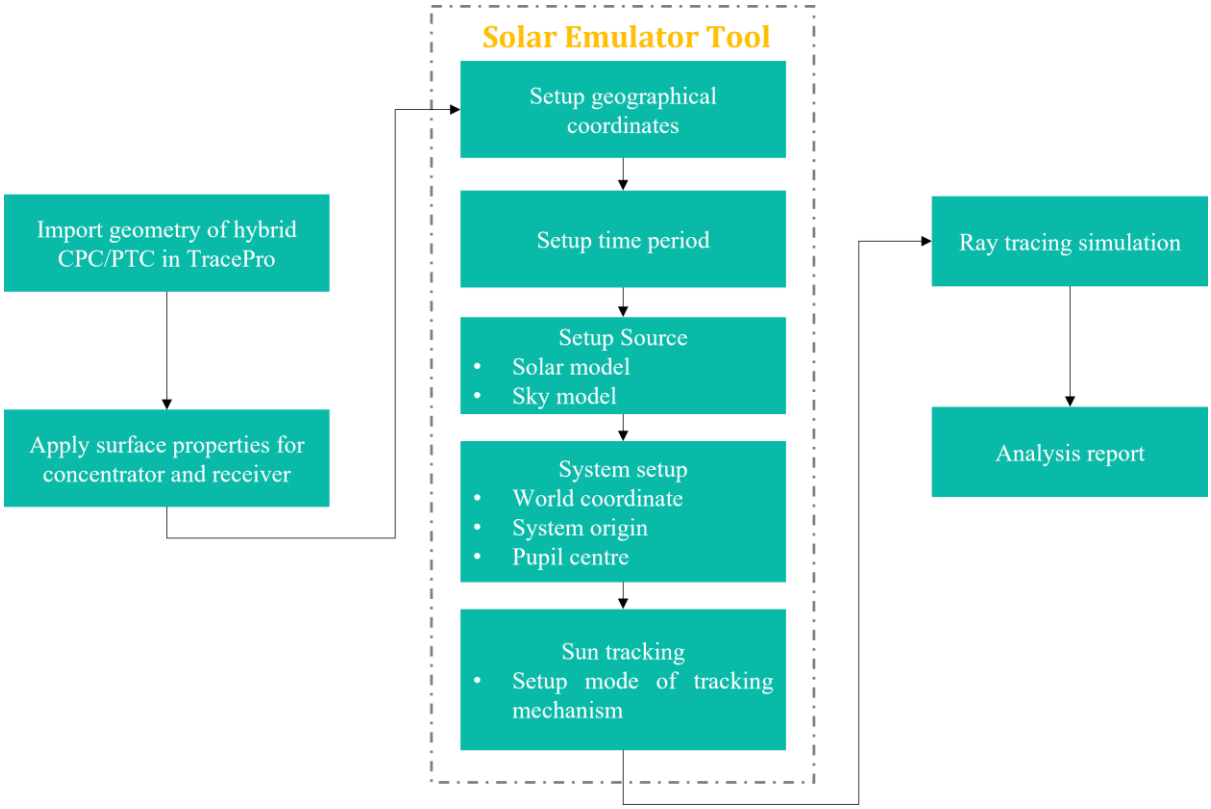

Fig. 8. Workflow of solar tracking in Solar Emulator tool

5. Model Validation

The accuracy of the Monte-Carlo ray-tracing model used in this study is validated using the findings of Zhang et al. [49], Karathanassis et al. [17] and Kasaeian et al. [50]. First, as shown in Fig. 9, the predicted transversal irradiance distribution on a CPC receiver is compared

to that predicted by Zhang et al. [49]. Second, Fig. 10 compares the predicted transversal irradiance distribution on a PTC receiver to the results obtained by Karathanassis et al. [17]. The comparisons show a strong agreement between the current study results and those obtained by Zhang et al. [49], with a maximum difference of about 2.26 % and a maximum difference of about 4.54 % when compared to the results estimated by Karathanassis et al. [17]. The intercept factor and optical efficiency are two critical parameters in optical modelling for validation. The TracePro simulation results are validated against the experimental results of Kasaeian et al. [50] to ensure its accuracy. Table 2 displays the validation results of the intercept factor and optical efficiency of a PTC from Kasaeian et al. [50].

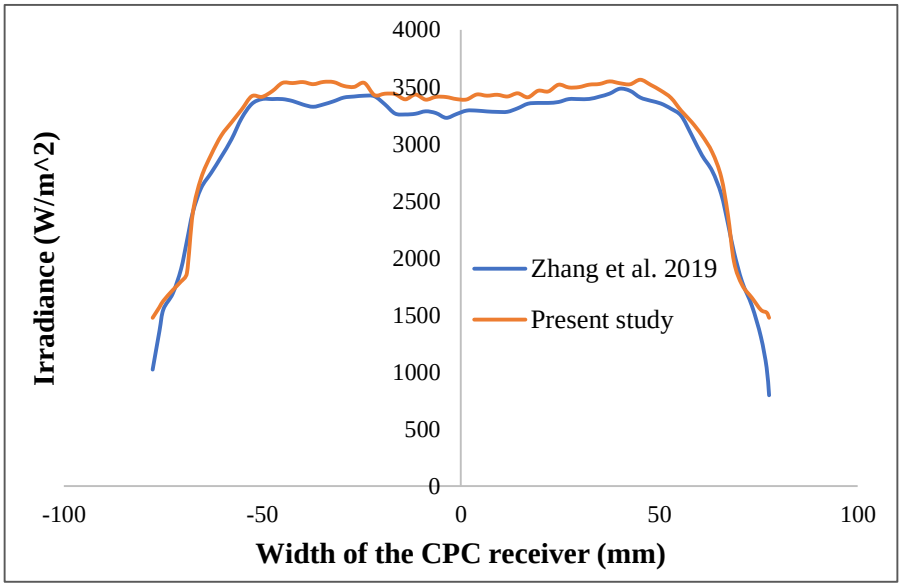

Fig. 9. The validation transversal profile of the irradiance distribution for CPC with a flat receiver

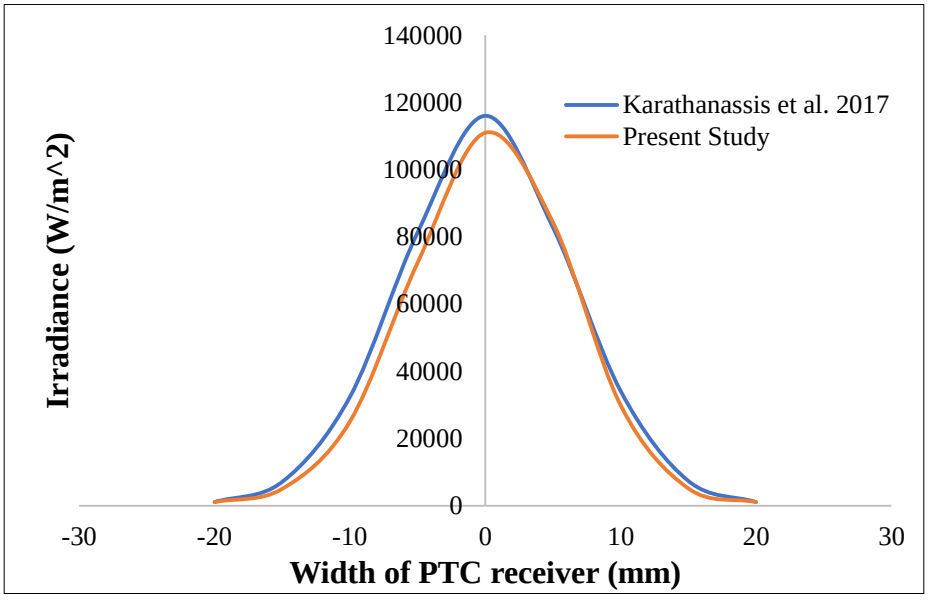

Fig. 10. The validation transversal profile of the irradiance distribution for PTC with a flat receiver

Table 2. Simulation results obtained using Tracepro software for validation

Parameters	Kasaeian et al. [50]	Present Study	Error (%)
Rim angle	90°	90°	-
Aperture width	0.7 m	0.7 m	-
length	2 m	2 m	-
Area	1.4 m^2	1.4 m^2	-
Receiver tube diameter	0.028 m	0.028 m	-
Glass tube diameter	0.06	0.06 m	-
Reflectivity of PTC	0.76	0.76	-
Transmissivity of the glass tube	0.9	0.9	-
Absorbance of receiver	0.98	0.98	-
Intercept factor	0.92	0.938	1.95
Optical efficiency	61.8	63	1.94

6. Results and Discussion

6.1 Optical Performance of CPC concentrator in hybrid CPC/PTC system

The irradiance distribution, non-uniformity and the optical efficiency of the full, HEMR and LEMR CPC concentrators are studied for different geometric concentration ratios varying from 2 to 8. The results are obtained by assuming a 0° incident angle in the ray-tracing simulation (i.e., fixed DNI source above the CPC aperture with incident rays parallel to the CPC axis).

6.1.1 Irradiance distribution of the CPC

The distribution of solar radiation received on the BCP is more homogeneous than the radiation received on the CPC outlet. The irradiation distribution of solar radiation received on the BCP of HEMR and LEMR CPCs with concentration ratios ranging from 2 to 8 is depicted in Figs. 11 and 12. The magnitude of the irradiance distribution on the receiver BCP increases as the concentration ratio increases in both types of CPCs. The magnitude of the two symmetrical peaks in the irradiance distribution gradually increases with increasing concentration ratio, indicating that irradiance distribution non-uniformity increases with increasing concentration ratio. It's also worth noting that the magnitude of the peaks in LEMR is higher than in HEMR for the same concentration ratio, implying that the LEMR CPCs irradiance distribution is more erratic than the HEMR CPCs. The degree of non-uniformity is determined from the standard deviation of the irradiance received on the individual pixels of the CPCs irradiance map. The dimensionless non-uniform factor is described as [49]:

$$\sigma_I = \frac{1}{I_{ref}} \sqrt{\frac{1}{n} \sum_{x=1}^{n} \left[I_{px}(x,y) - \bar{I}_{px} \right]^2} \tag{30}$$

where σ_I is the standard deviation non-uniform factor, I_{ref} is solar radiation under standard testing conditions, which is used to make σ_I a dimensionless factor, $I_{px}(x,y)$ is irradiance received on individual pixels, and $\bar{I}_{px}$ is the average of the irradiance received on all the pixels. The variation of irradiance non-uniformity of full, HEMR, and LEMR CPCs when received in outlet and BCP for various concentration ratios is depicted in Fig. 13. In general, the irradiance non-uniformity of three types of CPCs increases as the concentration ratio increases. Furthermore, the non-uniformity of the irradiance distribution of CPCs receiving irradiance at the outlet is greater than that of CPCs receiving irradiance on BCP. As a result, the HEMR CPC is assumed to be more uniform than the full and LEMR CPCs. The irradiance maps in Fig. 22 depict the solar irradiance distribution received for 0° incident angle at the outlet and BCP of Full, HEMR, and LEMR CPCs (see Appendix A).

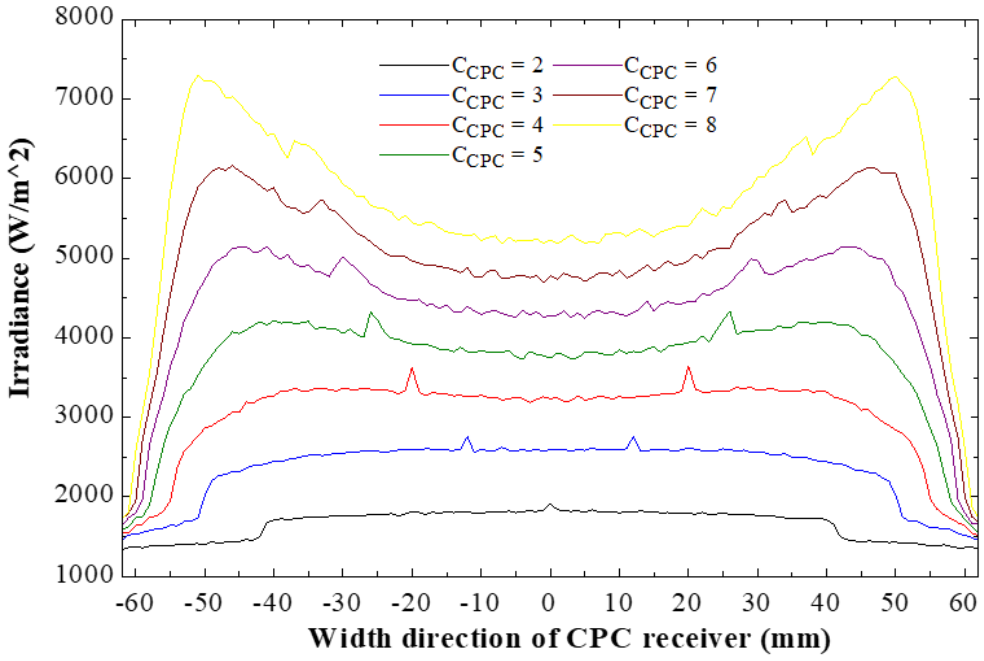

Fig. 11. Irradiance distribution of HEMR CPC

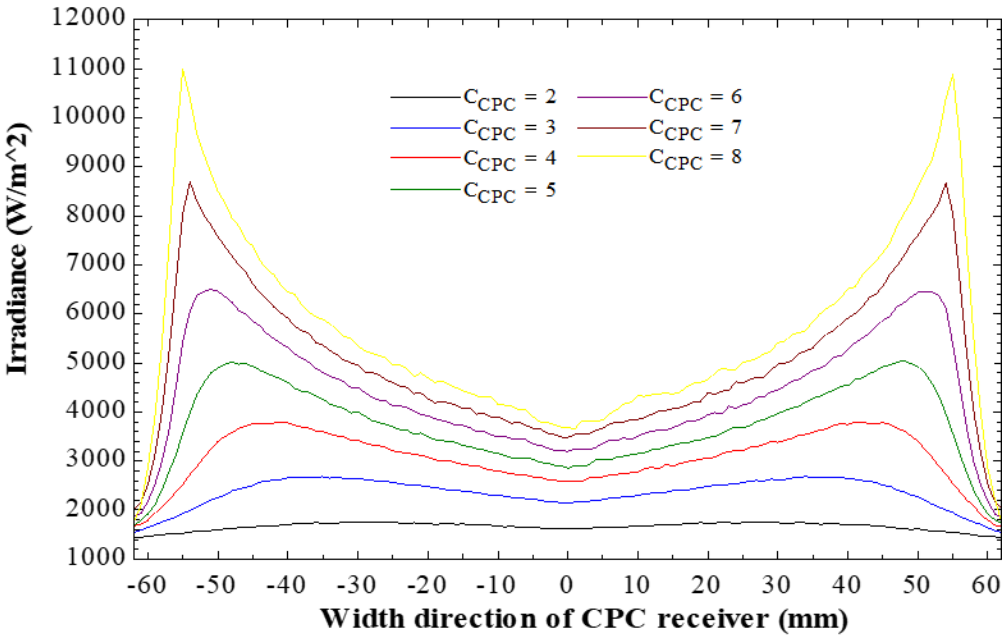

Fig. 12. Irradiance distribution of LEMR CPC

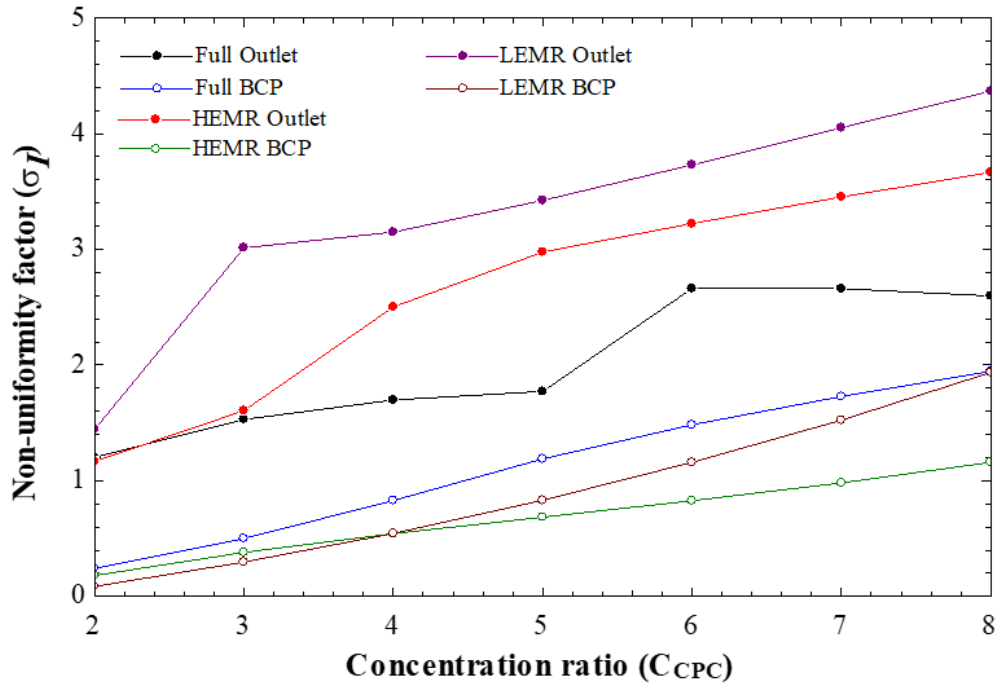

Fig. 13. Irradiance non-uniformity versus concentration ratio for different CPCs

6.1.2 Optical efficiency of CPC

The ray-tracing simulation is used to calculate the amount of irradiance received on the CPCs' outlet aperture and BCP. The optical efficiency of full, HEMR, and LEMR CPCs is calculated using Eq. (18). When the incident angle is 0°, Fig. 14 depicts the optical efficiency at the outlet aperture and BCP of CPCs at different concentration ratios. The optical efficiency of CPCs is found to decrease as the concentration ratio increases. Because full CPCs have

optical losses due to numerous reflections, their optical efficiency is lower than that of HEMR and LEMR CPCs.

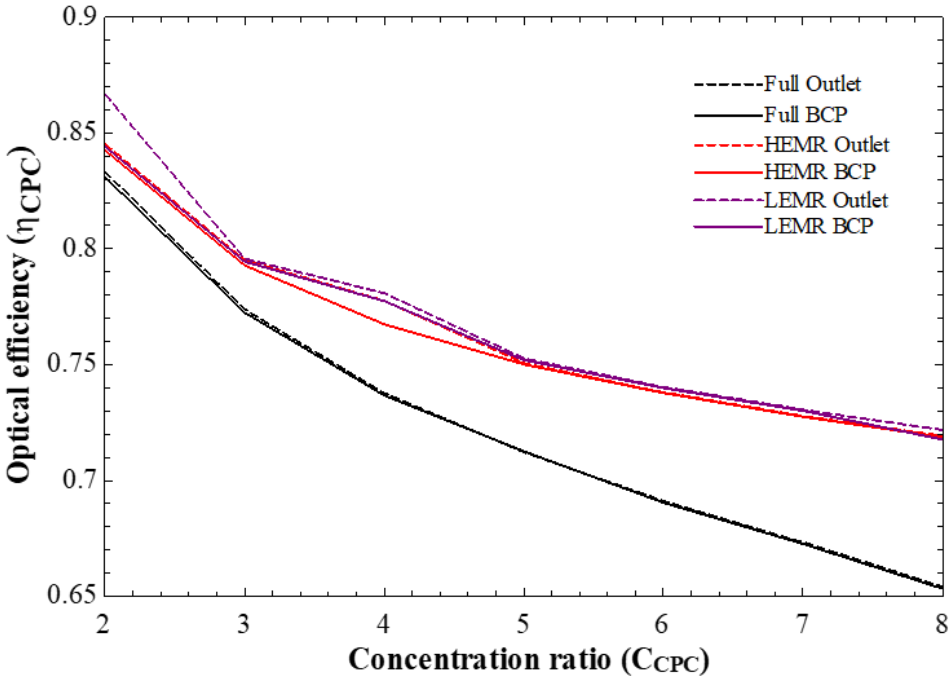

Fig. 14. The optical efficiency of different CPCs for different concentration ratios

6.2 Optical performance of PTC in hybrid CPC/PTC system

A hybrid CPC/PTC system with 4 HEMR CPC is considered to study the optical performance of the PTC and the overall optical efficiency of the hybrid CPC/PTC system. The intercept factor, image width, concentration ratio, and optical efficiency of PTC in a hybrid CPC/PTC system are investigated for various rim angles and aperture widths. The intercept factor is a critical parameter in determining the optical efficiency of PTC. For various rim angles, Fig. 15 depicts the relationship between the intercept factor and the PTC aperture width. As shown in the figure, the intercept factor increases as the rim angle increases. In addition, as the aperture width of the PTC increases, so does the intercept factor. PTC with a rim angle of 75° and aperture width of 6 m has the highest intercept factor of 0.87. When the aperture width is 1 m, the intercept factor is less than 0.5 for rim angles ranging from 15° to 75°.

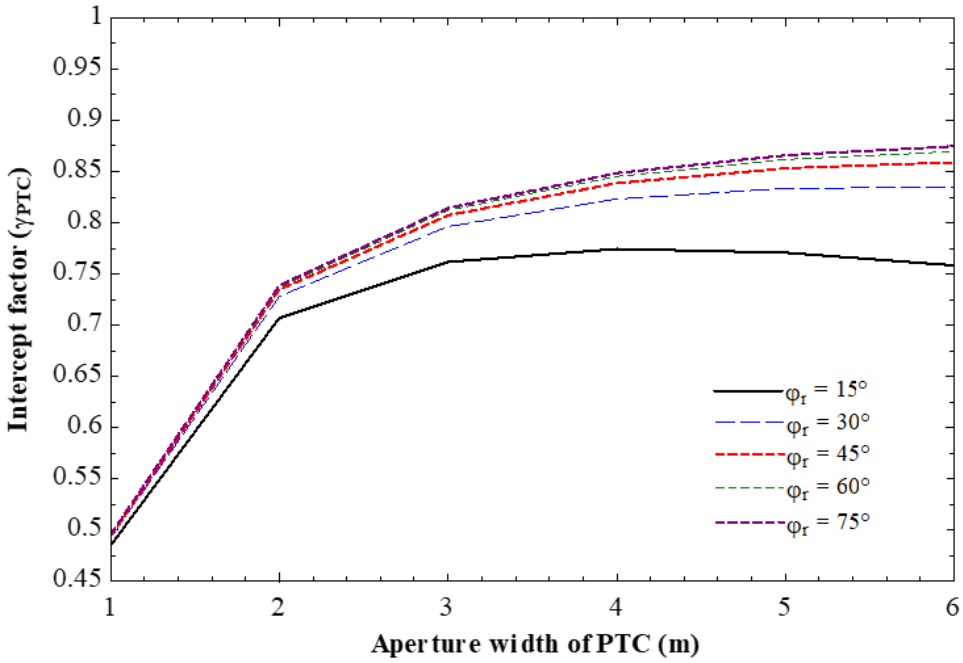

Fig. 15. The relation between intercept factor and aperture width for various rim angle

Another crucial optical parameter is the image width formed by the PTC on the flat receiver. Fig. 16 shows that for various rim angles, the image width increases linearly with increasing aperture width. Fig. 16 also indicates that the image width formed by PTCs with rim angles 15° and 75° is equal; similarly, the image width of PTCs with rim angles 30° and 60° is equal. It is also evident from Fig. 16 that the image width of PTC with a 45° rim angle is smaller when compared to other rim angles. This proves that the maximum concentration ratio is obtained for a PTC with a flat receiver when the rim angle is 45°.

Table 3 compares the concentration ratio of PTC in the hybrid CPC/PTC system and the concentration ratio of standard PTC for various aperture widths and the rim angles. It is observed from Table 3 that the concentration ratio is maximum when the rim angle is 45°. It is also observed from Table 3 that the concentration ratio of PTC in hybrid CPC/PTC is almost half of the concentration ratio of standard PTC when the aperture width is 1m; this loss in concentration ratio is mainly because of the shadow of the CPC on the PTC. As displayed in Table 3 for a CPC/PTC system with fixed CPC, the loss in the PTC concentration ratio can be reduced by increasing the aperture width of the PTC. For example, when the aperture width of PTC is 1 m (45° rim angle), the concentration ratio of PTC in the CPC/PTC system is 49.5 % lower than standard PTC. On the other hand, when the aperture width is 6 m (45° rim angle), the difference between the concentration ratio of PTC in CPC/PTC and standard PTC is reduced to 7.5 %.

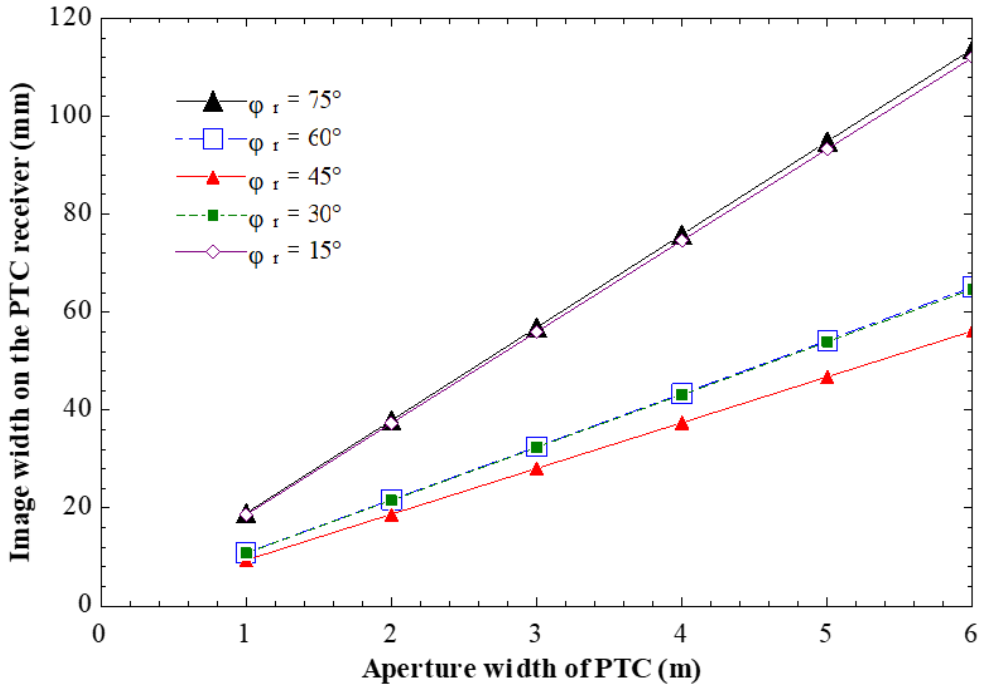

Fig. 16. The variation of image width with aperture width for various rim angle

Table 3. Comparison of concentration ratio of Standard PTC with PTC in hybrid CPC/PTC

Rim angle	**15 Deg**		**30 Deg**		**45 Deg**		**60 Deg**		**75 deg**	
Width	CR of Standard PTC	CR of PTC in CPC/PTC	CR of Standard PTC	CR of PTC in CPC/PTC	CR of Standard PTC	CR of PTC in CPC/PTC	CR of Standard PTC	CR of PTC in CPC/PTC	CR of Standard PTC	CR of PTC in CPC/PTC
1 m	46.9	23.9	83.08	41.98	96.18	48.48	83.15	42	47.21	24.04
2 m	45.53	34.84	81.83	62.03	95.27	72.1	82.43	62.47	46.84	35.79
3 m	44.2	37.53	80.58	67.87	94.27	79.27	81.71	68.81	46.47	39.46
4 m	42.82	38.17	79.33	70.16	93.23	82.32	81	71.62	46.11	41.11
5 m	41.42	37.98	78.07	71.02	92.22	83.76	80.27	73.02	45.74	41.95
6 m	40.03	37.38	76.8	71.16	91.24	84.37	79.55	73.7	45.39	42.39

6.3 Optical efficiency of hybrid CPC/PTC system

The optical efficiency of the hybrid CPC/PTC is calculated using Eq. (18-25). The comparison of the standard PTC's optical efficiency with the hybrid CPC/PTC system for various rim angles and aperture width is shown in Table 4. As displayed in Table 4, the maximum overall optical efficiency achieved by the hybrid CPC/PTC system is ~73% for 1m aperture width, which is ~6.35 % higher than standard PTC. Also, raising the rim angle from 15° to 75° improves optical performance slightly. For different aperture widths (1m – 6m), the concentration ratio of a standard PTC is compared to the concentration ratio of the PTC integrated with the hybrid CPC/PTC system in Table 3. The analysis revealed that in a hybrid CPC/PTC system with a CPC having a fixed aperture area, the loss in the PTC concentration ratio caused by the CPC decreases as the aperture width increases. As a result, the optical

efficiency of the PTC in the hybrid CPC/PTC system increases as the aperture width increases (See Fig. 17). However, the overall optical efficiency (combined efficiency of CPC and PTC) of the hybrid CPC/PTC decreases slightly as the aperture width increases (see Table 4 & Fig. 17). This slight decrease in optical efficiency as aperture width increases is primarily due to the effect of CPC on the PTC. Regardless of the rim angle and aperture width, the hybrid CPC/PTC system has a higher overall efficiency than standard PTC.

Table 4. Comparison of optical efficiency of standard PTC with hybrid CPC/PTC for various rim angle and aperture width of PTC

Rim angle	**15 Deg**		**30 Deg**		**45 Deg**		**60 Deg**		**75 deg**	
Width	Optical efficiency of Standard PTC	Optical efficiency of CPC/PTC	Optical efficiency of Standard PTC	Optical efficiency of CPC/PTC	Optical efficiency of Standard PTC	Optical efficiency of CPC/PTC	Optical efficiency of Standard PTC	Optical efficiency of CPC/PTC	Optical efficiency of Standard PTC	Optical efficiency of CPC/PTC
1 m	66.84	72.41	68.33	72.89	68.64	72.97	68.76	73.10	68.26	73.13
2 m	64.77	68.75	67.30	70.20	68	70.65	68.17	70.84	67.73	70.93
3 m	62.88	66.18	66.27	68.61	67.27	69.36	67.57	69.7	67.20	69.84
4 m	60.91	63.89	65.24	67.29	66.54	68.35	66.98	68.82	66.67	69.03
5 m	58.92	61.71	64.21	66.08	65.81	67.45	66.38	68.05	66.14	68.33
6 m	56.95	59.59	63.17	64.93	65.08	66.61	65.79	67.34	65.61	67.68

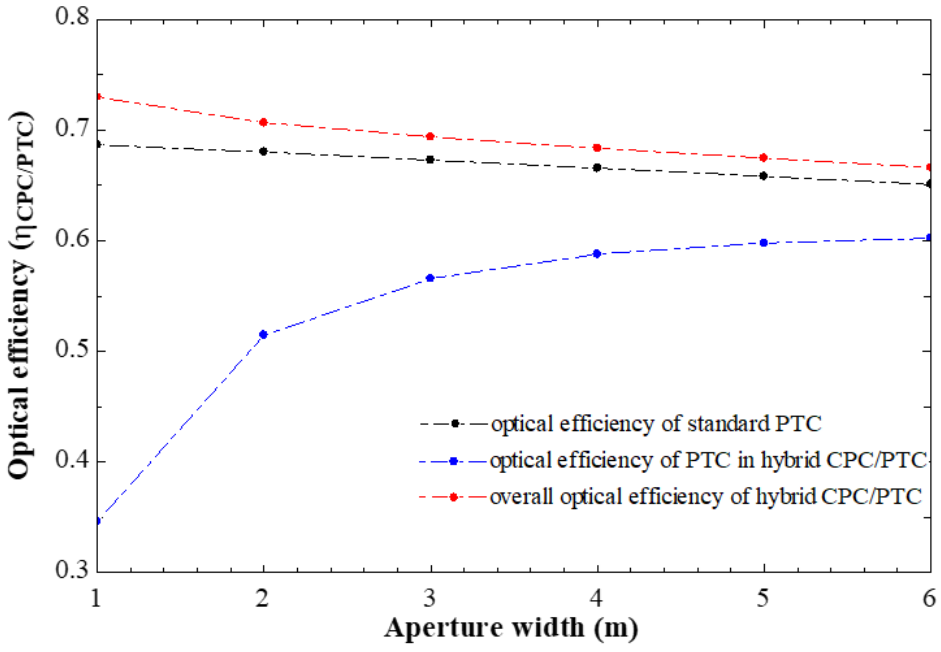

Fig. 17. Comparison of optical efficiency of standard PTC, PTC in CPC/PTC and hybrid CPC/PTC system (45° rim angle)

6.4 Optical efficiency of CPC/PTC under different modes of tracking

The solar radiation received on the days of the equinox (20th March), summer solstice (21st June), and winter solstice (21st December) in the year 2020 was used to simulate the optical performance of the hybrid CPC/PTC system under different tracking modes. Accuracy of tracking is essential when we consider tracking in solar concentrators for maximum optical efficiency. In the present study, the effect of modes of tracking on the optical efficiency of hybrid CPC/PTC system in proportional to the incidence angle's cosine is analysed; hence the tracking error is presumed to be zero. From Fig. 18, it was observed that the dual-axis tracking has almost constant optical efficiency from morning to evening during the equinox, summer and winter solstices. It is because of the 0° incident angle in the dual-axis tracking mode. The dual-axis tracking mode can achieve higher optical efficiency of ~70% at all sun positions. In the east-west tracking on a north-south polar axis, the maximum optical efficiency is obtained during equinox because the sun will be normal to the concentrator (See Fig.19). From Fig. 19 its also observed that the optical performance during summer and winter solstices is equal and less compared with the performance during the equinox. The drop in efficiency during solstices is caused by an increase in incident angle, which increases the loss due to the cosine effect. The optical efficiency is highest at noon when the incident angle is 0° and decreases in the morning and evening due to cosine and end losses, as shown in Fig. 20. The optical performance of the east-west tracking mode on a horizontal north-south axis is similar to the east-west tracking mode on a polar north-south axis (see Fig. 21).

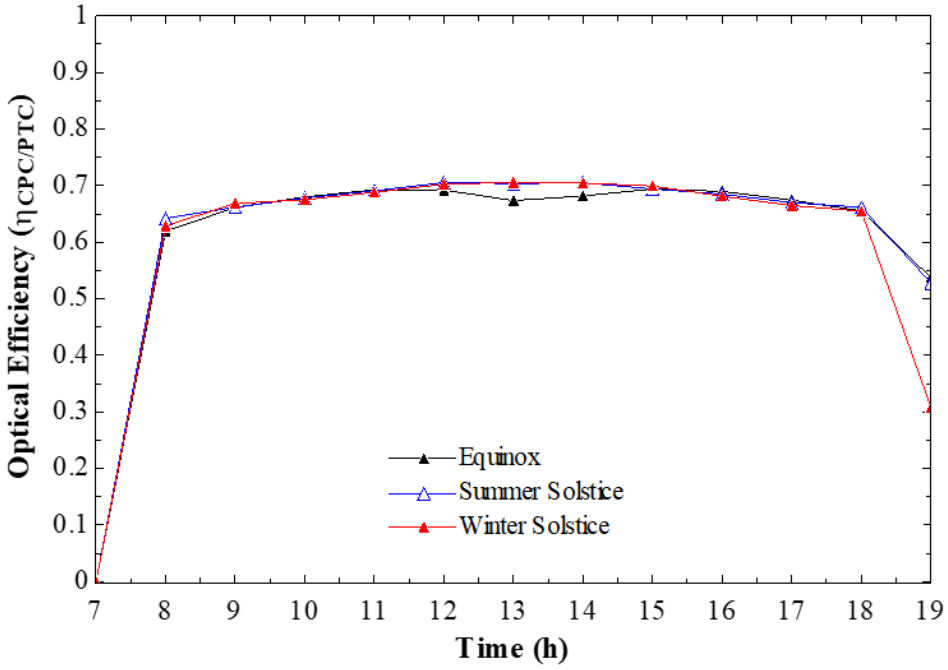

Fig. 18. Optical efficiency of hybrid CPC/PTC: dual-axis tracking

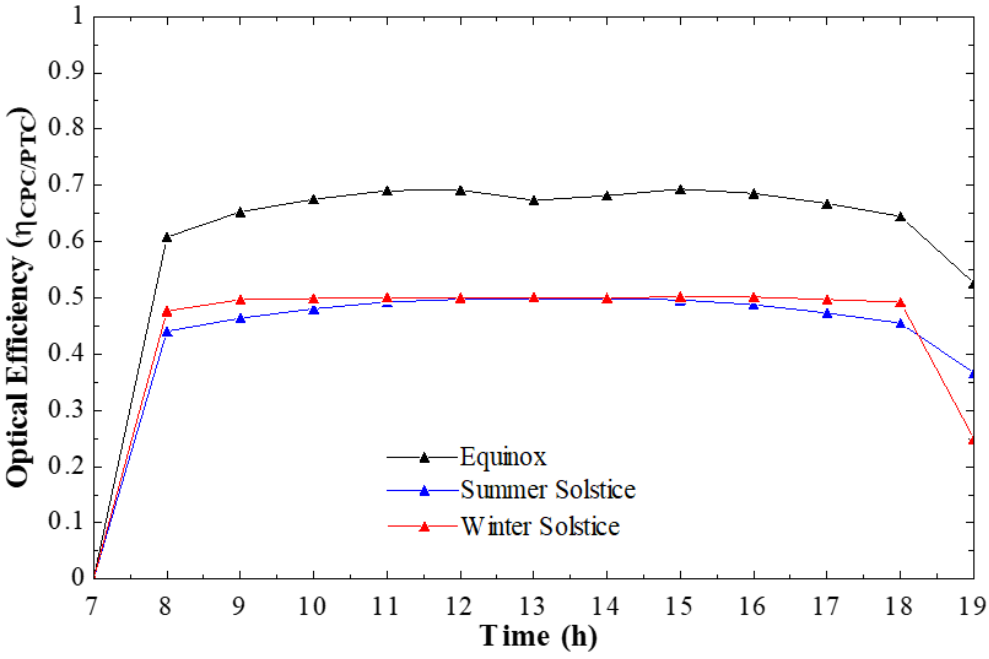

Fig. 19. Optical efficiency of hybrid CPC/PTC: E-W tracking on a N-S polar axis

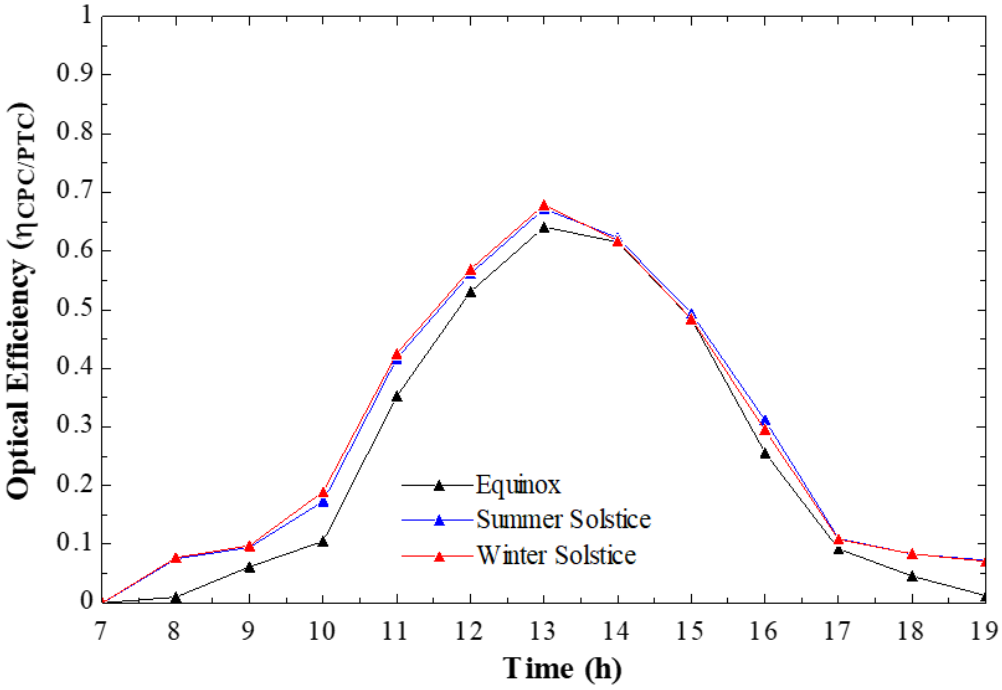

Fig. 20. Optical efficiency of hybrid CPC/PTC: N-S tracking on a horizontal E-W axis

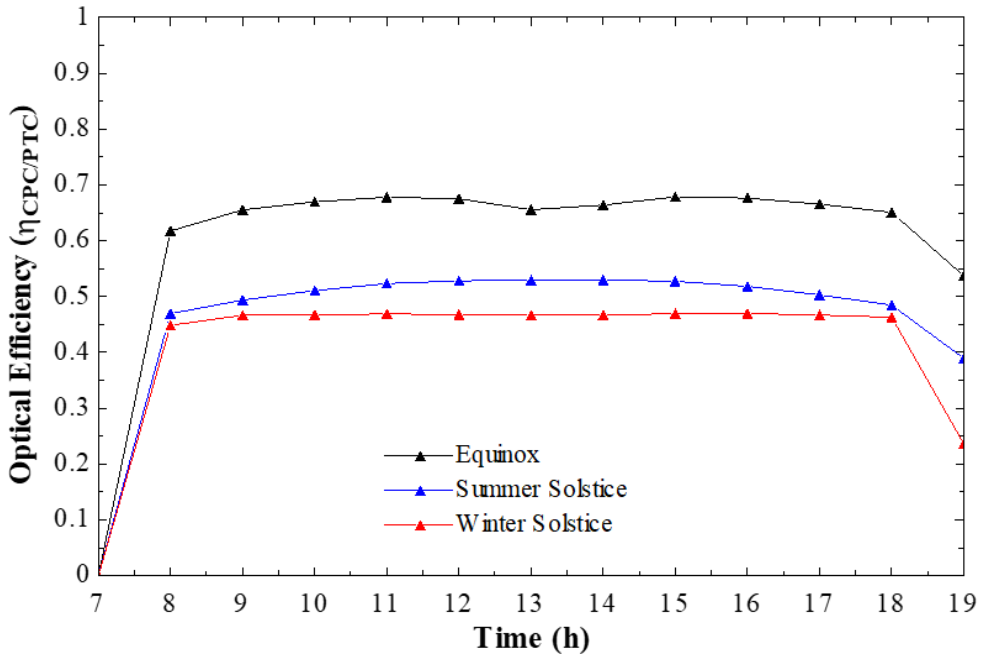

Fig. 21. Optical efficiency of hybrid CPC/PTC: E-W tracking on a horizontal N-S axis

The mode of tracking affects the optical efficiency of the hybrid CPC/PTC system with respect to the cosine of the incident angle. The amount of solar energy received by CPC/PTC from morning to evening for the equinox, summer and winter solstices are given in Table 5. The performance of the different tracking modes is correlated with dual-axis tracking, which receives the maximal of solar radiation, indicated as 100 % in Table 5. This table shows that

the hybrid CPC/PTC with dual-axis tracking mode receives maximum solar energy of 27.82 kWh, 27.68 kWh and 26.488 kWh during the equinox, summer solstice, and winter solstice. It is also evident that the polar axis with east-west tracking and horizontal north-south axis with east-west tracking is more suitable for single-axis tracking.

Table 5. Comparison of solar energy received by the hybrid CPC/PTC system for different tracking modes

Tracking Mode	Energy Received (kWh)			Percentage to dual-axis tracking		
	Equinox	Summer solstice	Winter Solstice	Equinox	Summer solstice	Winter Solstice
Dual axis	27.82	27.68	26.488	100	100	100
E-W tracking on a N-S polar axis	27.662	19.548	19.301	99.4	70.6	72.8
N-S tracking on a horizontal E-W axis	13.241	14.424	14.186	47.6	52.1	53.5
E-W tracking on a horizontal N-S axis	27.315	20.786	18.072	98.1	75.1	68.2

7. Conclusion

Optical performance is one of the crucial factors that affect the performance of a solar concentrator system. Therefore, the optical performance of a novel CPC/PTC hybrid system is investigated using Monte-Carlo ray-tracing simulation for various rim angles and aperture widths. The corresponding outcomes are as follows :

- At first, the irradiance distribution, non-uniformity, and optical efficiency of HEMR and LEMR CPCs with flat receivers were studied for different concentration ratios ranging from 2 – 8. The results revealed that the uniformity of irradiance distribution in HEMR CPC is greater than that in LEMR CPC. Furthermore, as the concentration ratio increases, so does the non-uniformity in CPCs. The optical efficiency of the CPC, on the other hand, decreases as the concentration ratio increases.
- A hybrid CPC/PTC system with 4 CR HEMR CPC is considered, and its impact on the optical performance of the PTC is evaluated. The PTC intercept factor is found to increase as the rim angle and aperture width increase.
- The maximum CR for the PTC with the flat receiver is obtained when the rim angle is 45°. The CR of the PTC in the CPC/PTC hybrid system is compared with the standard PTC CR. The results showed that for a hybrid CPC/PTC with fixed CPC, the reduction in CR of the PTC due to the top CPC's shadow is reduced when the aperture width of the PTC is increased.

- The maximum calculated optical efficiency of the hybrid CPC/PTC system is ~73% which is ~6.35% higher than standard PTC.
- Finally, the proposed hybrid CPC/PTC system's optical efficiency is evaluated under various tracking modes for equinox, summer solstice, and winter solstice. The results verified that the dual-axis tracking CPC/PTC achieves maximum efficiency of ~70% on the equinox, summer and winter solstices. Furthermore, compared with other tracking modes, the dual-axis tracking CPC/PTC system receives a maximum of 27.82 kWh of solar energy during the equinox.

Existing PTC based power plants can be retrofitted as CPVT and CPVT/TEG power plants using the proposed novel design. The present work focused only on the optical performance of the hybrid CPC/PTC system. Therefore, there is a need for future works on the hybrid CPC/PTC system's electrical, thermal and economic performance. The optical results of the current study can be used in the electrical and thermal analysis of hybrid CPC/PTC based CPVT and CPV/T-TEG systems.

Acknowledgement

Taylor's University supported this work through its TAYLOR'S PhD SCHOLARSHIP Programme and Taylor's University Flagship Research Grant (TUFR/2017/001/01).

Appendix A: Irradiance Map showing distribution of solar irradiance at the outlet and BCP of different types of CPCs

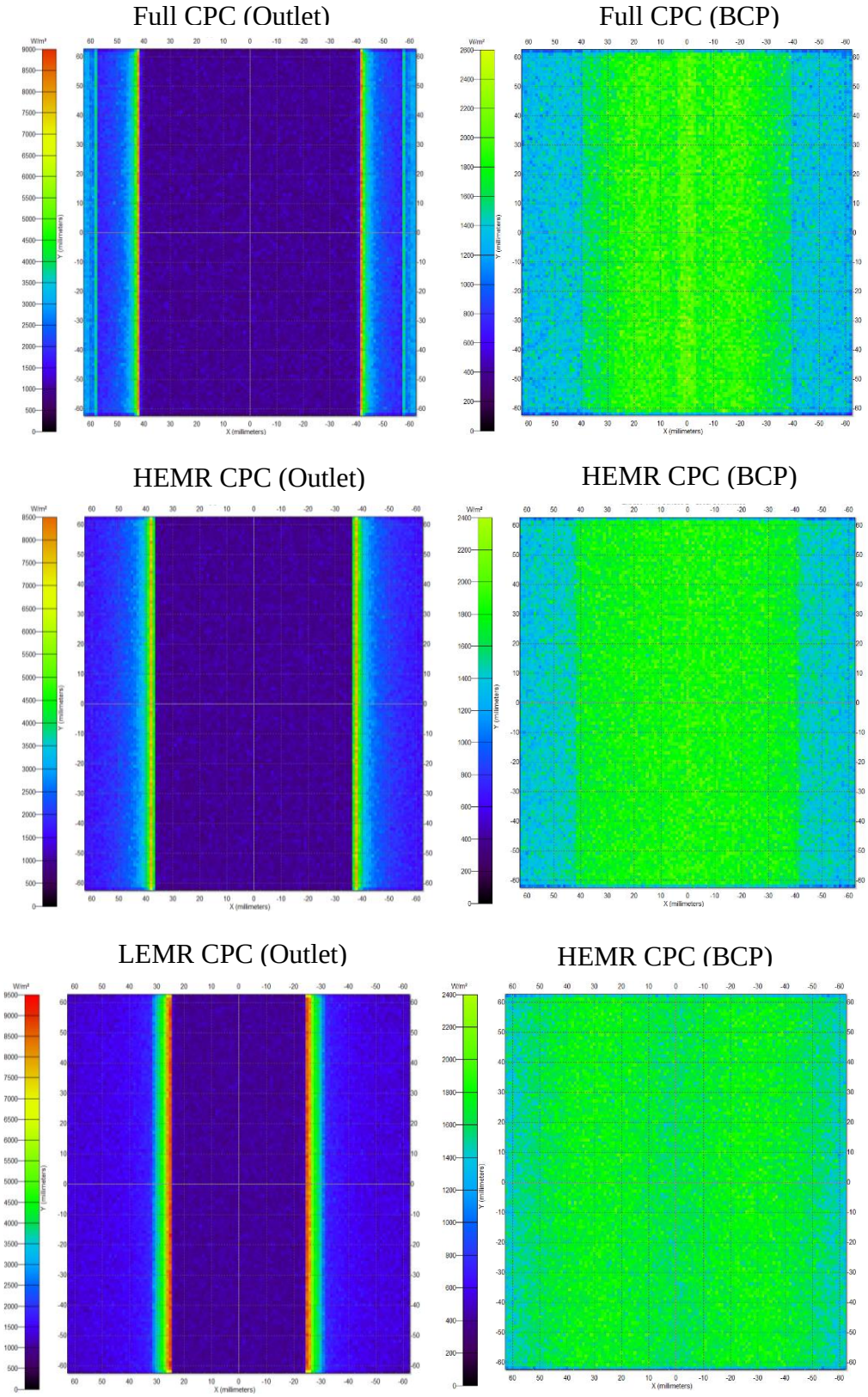

Fig. 22. Irradiance map of distribution of solar flux received at the Outlet and BCP of Full, HEMR and LEMR CPCs when the incident angle is 0°.

Annexure B: The graphical user interface (GUI) of Solar Emulator Tool

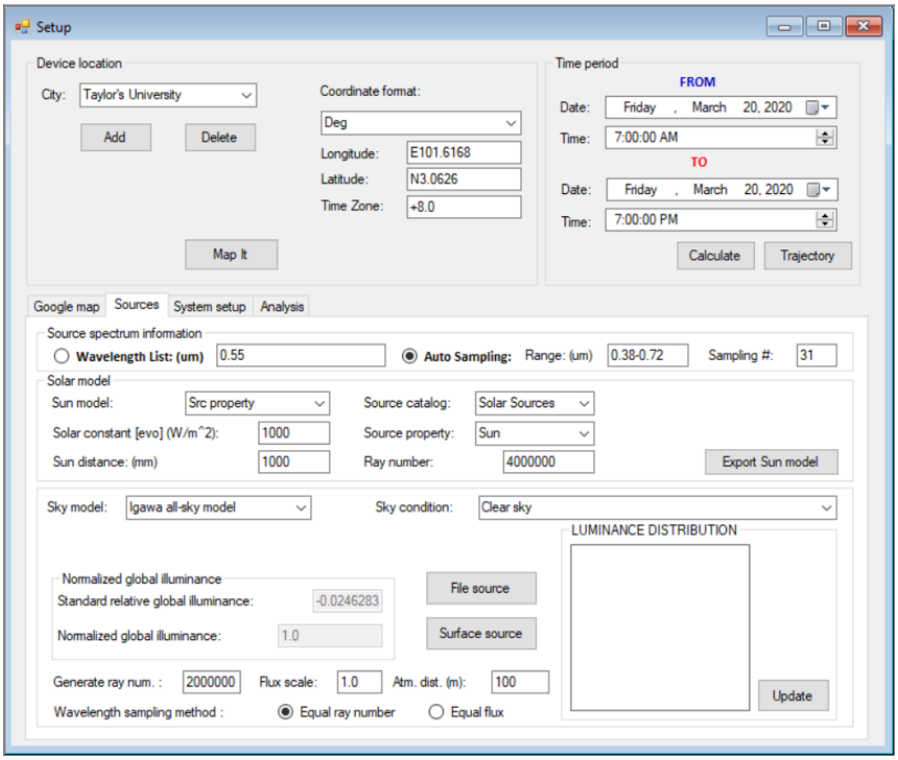

(a)

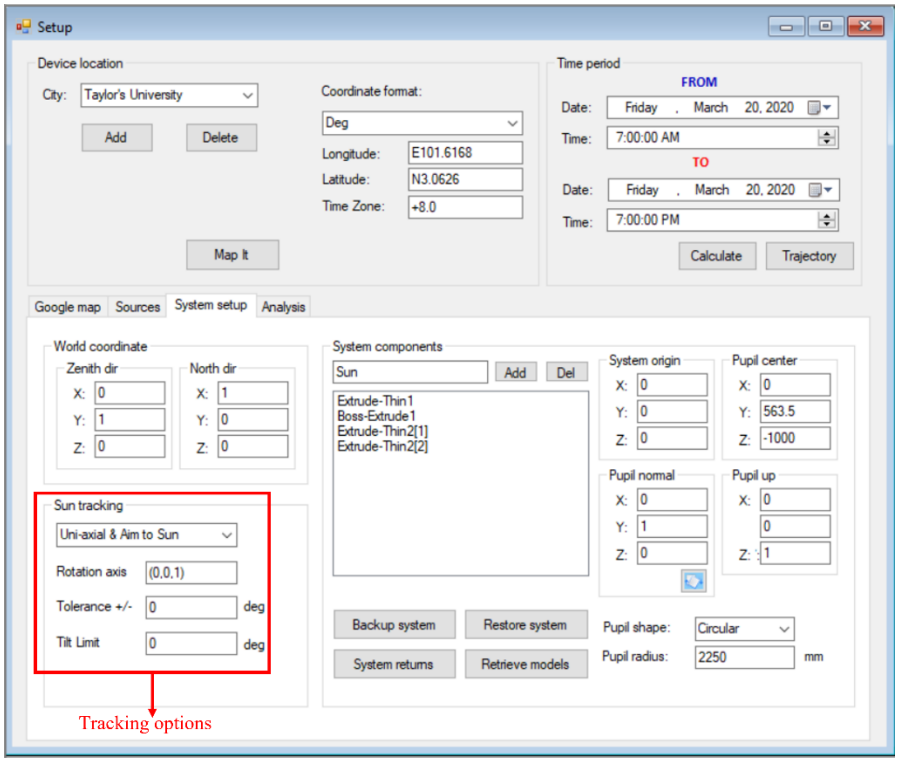

(b)

Fig. 23. The GUI of the Solar Emulator tool showing; (a) source setup (b) system setup

References

[1] Inernational Energy Agency. World Energy Outlook 2020. 2020.

[2] Shittu S, Li G, Akhlaghi YG, Ma X, Zhao X, Ayodele E. Advancements in thermoelectric generators for enhanced hybrid photovoltaic system performance. Renew Sustain Energy Rev 2019;109:24–54. doi:10.1016/j.rser.2019.04.023.

[3] Li G, Shittu S, Diallo TMO, Yu M, Zhao X, Ji J. A review of solar photovoltaic-thermoelectric hybrid system for electricity generation. Energy 2018;158:41–58. doi:10.1016/j.energy.2018.06.021.

[4] Allouhi A. Advances on solar thermal cogeneration processes based on thermoelectric devices: A review. Sol Energy Mater Sol Cells 2019;200:109954. doi:10.1016/j.solmat.2019.109954.

[5] Sripadmanabhan Indira S, Vaithilingam CA, Chong KK, Saidur R, Faizal M, Abubakar S, et al. A review on various configurations of hybrid concentrator photovoltaic and thermoelectric generator system. Sol Energy 2020;201:122–48. doi:10.1016/j.solener.2020.02.090.

[6] Daneshazarian R, Cuce E, Cuce PM, Sher F. Concentrating photovoltaic thermal (CPVT) collectors and systems: Theory, performance assessment and applications. Renew Sustain Energy Rev 2018;81:473–92. doi:10.1016/j.rser.2017.08.013.

[7] Luque A, Andreev VM. Concentrator Photovoltaics. Springer; 2007.

[8] Gibart C. Study of and tests on a hybrid photovoltaic-thermal collector using concentrated sunlight. Sol Cells 1981;4:71–89.

[9] Chenlo F, Cid M. A linear concentrator photovoltaic module: analysis of non-uniform illumination and temperature effects on efficiency. Sol Cells 1987;20:27–39. doi:10.1016/0379-6787(87)90018-4.

[10] Chemisana D, Ibáñez M, Barrau J. Comparison of Fresnel concentrators for building integrated photovoltaics. Energy Convers Manag 2009;50:1079–84. doi:10.1016/j.enconman.2008.12.002.

[11] Chemisana D, Ibáñez M, Rosell JI. Characterization of a photovoltaic-thermal module for Fresnel linear concentrator. Energy Convers Manag 2011;52:3234–40. doi:10.1016/j.enconman.2011.04.008.

[12] Kasaeian A, Tabasi S, Ghaderian J, Yousefi H. A review on parabolic trough/Fresnel based photovoltaic thermal systems. Renew Sustain Energy Rev 2018;91:193–204. doi:10.1016/j.rser.2018.03.114.

[13] Nilsson J, Hakansson H, Karlsson B. Electrical and thermal characterisation of a PV-CPC hybrid. Sol Energy 2007;81:917–28. doi:10.1016/j.solener.2006.11.005.

[14] Chaabane M, Charfi W, Mhiri H, Bournot P. Performance evaluation of concentrating solar photovoltaic and photovoltaic/thermal systems. Sol Energy 2013;98:315–21. doi:10.1016/j.solener.2013.09.029.

[15] Coventry JS. Performance of a concentrating photovoltaic/thermal solar collector. Sol Energy 2005;78:211–22. doi:10.1016/j.solener.2004.03.014.

[16] Yongfeng X, Ming L, Liuling W, Wenxian L, Ming X, Xinghua Z, et al. Performance analyss of solar cell arrays in concentrating light intensity. J Semicond 2009;30:1–6. doi:10.1088/1674-4926/30/8/084011.

[17] Karathanassis IK, Papanicolaou E, Belessiotis V, Bergeles GC. Design and experimental evaluation of a parabolic-trough concentrating photovoltaic/thermal (CPVT) system with high-efficiency cooling. Renew Energy 2017;101:467–83. doi:10.1016/j.renene.2016.09.013.

[18] Li M, Ji X, Li G, Wei S, Li Y, Shi F. Performance study of solar cell arrays based on a Trough Concentrating Photovoltaic / Thermal system. Appl Energy 2011;88:3218–27. doi:10.1016/j.apenergy.2011.03.030.

[19] Li M, Li GL, Ji X, Yin F, Xu L. The performance analysis of the Trough Concentrating Solar Photovoltaic/Thermal system. Energy Convers Manag 2011;52:2378–83. doi:10.1016/j.enconman.2010.12.039.

[20] Saleh Ali IM, O'Donovan TS, Reddy KS, Mallick TK. An optical analysis of a static 3-D solar concentrator. Sol Energy 2013;88:57–70. doi:10.1016/j.solener.2012.11.004.

[21] Sellami N, Mallick TK. Optical efficiency study of PV Crossed Compound Parabolic Concentrator. Appl Energy 2013;102:868–76. doi:10.1016/j.apenergy.2012.08.052.

[22] Li G, Pei G, Yang M, Ji J, Su Y. Optical evaluation of a novel static incorporated compound parabolic concentrator with photovoltaic/thermal system and preliminary experiment. Energy Convers Manag 2014;85:204–11. doi:10.1016/j.enconman.2014.05.082.

[23] Kamnapure NR, Reddy KS. Optical analysis of solar parabolic trough collector with flat concentrating photovoltaic receiver. Appl Mech Mater 2014;592–594:2396–403. doi:10.4028/www.scientific.net/AMM.592-594.2396.

[24] Abdullahi B, AL-Dadah RK, Mahmoud S, Hood R. Optical and thermal performance of double receiver compound parabolic concentrator. Appl Energy 2015;159:1–10. doi:10.1016/j.apenergy.2015.08.063.

[25] Rehman N ur, Uzair M, Siddiqui MA. Optical analysis of a novel collector design for a solar concentrated thermoelectric generator. Sol Energy 2018;167:116–24. doi:10.1016/j.solener.2018.03.087.

[26] Khalid M, Wei J, Zhang G, Xie H, Fang J, Qaisrani MA, et al. Optical performance of quasi-stationary, low-concentration, and low-profile compound parabolic concentrators. J Renew Sustain Energy 2019;11. doi:10.1063/1.5109447.

[27] Beeri O, Rotem O, Hazan E, Katz EA, Braun A, Gelbstein Y. Hybrid photovoltaic-thermoelectric system for concentrated solar energy conversion: Experimental realisation and modeling. J Appl Phys 2015;118. doi:10.1063/1.4931428.

[28] Lashin A, Turkestani M Al, Sabry M. Concentrated photovoltaic/thermal hybrid system coupled with a thermoelectric generator. Energies 2019;12:1–12. doi:10.3390/en12132623.

[29] Bjørk R, Nielsen KK. The performance of a combined solar photovoltaic (PV) and thermoelectric generator (TEG) system. Sol Energy 2015;120:187–94. doi:10.1016/j.solener.2015.07.035.

[30] Abdo A, Ookawara S, Ahmed M. Performance evaluation of a new design of concentrator photovoltaic and solar thermoelectric generator hybrid system. Energy Convers Manag 2019;195:1382–401. doi:10.1016/j.enconman.2019.04.093.

[31] Corporation LR. TracePro User's Manual. Littleton, MA 01460: 2019.

[32] Wang J, Yang S, Jiang C, Yan Q, Lund PD. A novel 2-stage dish concentrator with improved optical performance for concentrating solar power plants. Renew Energy 2017;108:92–7. doi:10.1016/j.renene.2017.02.059.

[33] Gong J, Jin W, Xu Z, Huang B, Wang J, Wang C. Numerical study on the uniformity of reflective high concentration photovoltaic system with two-stage reflective concentrator. Sol Energy 2020;199:206–13. doi:10.1016/j.solener.2020.01.089.

[34] Khalifa AJN, Al-Mutawalli SS. Effect of two-axis sun tracking on the performance of compound parabolic concentrators. Energy Convers Manag 1998;39:1073–9. doi:10.1016/S0196-8904(97)10020-6.

[35] Kim Y, Han GY, Seo T. An evaluation on thermal performance of CPC solar collector. Int Commun Heat Mass Transf 2008;35:446–57. doi:10.1016/j.icheatmasstransfer.2007.09.007.

[36] Duffie JA, Beckman WA. Solar Engineering of Thermal Processes. Fourth ed. 2013.

[37] Kalogirou SA. Solar Energy Engineering Processes and Systems. 2nd ed. 2014.

[38] Xie H, Wei J, Wang Z, Liu Z, Gao Y, Ma Q, et al. Design and performance study of truncated CPC by eliminating multiple reflections of solar radiation in hybrid CPV/T system: Highest and lowest truncation position. Sol Energy 2016;136:217–25. doi:10.1016/j.solener.2016.06.077.

[39] Xie H, Wei J, Wang Z, Yang G, Ma Q. Design and performance research on eliminating multiple reflections of solar radiation within compound parabolic concentrator (CPC) in hybrid CPV/T system. Sol Energy 2016;129:126–46. doi:10.1016/j.solener.2016.01.037.

[40] Rodriguez-Sanchez D, Rosengarten G. Improving the concentration ratio of parabolic troughs using a second-stage flat mirror. Appl Energy 2015;159:620–32. doi:10.1016/j.apenergy.2015.08.106.

[41] Chaves J. Introduction to Non-Imaging Optics. CRC Press, Taylor & Francis Group; 2008.

[42] Azzouzi D, Bourorga H eddine, Belainine K abdelrahim, Boumeddane B. Experimental study of a designed solar parabolic trough with large rim angle. Renew Energy 2018;125:495–500. doi:10.1016/j.renene.2018.01.041.

[43] Behar O, Khellaf A, Mohammedi K. A novel parabolic trough solar collector model – Validation with experimental data and comparison to Engineering Equation Solver (EES). ENERGY Convers Manag 2015;106:268–81. doi:10.1016/j.enconman.2015.09.045.

[44] Yang S, Wang J, Lund PD, Jiang C, Liu D. Assessing the impact of optical errors in a novel 2-stage dish concentrator using Monte-Carlo ray-tracing simulation. Renew Energy 2018;123:603–15. doi:10.1016/j.renene.2018.02.034.

[45] Li Z, Tang D, Du J, Li T. Study on the radiation flux and temperature distributions of the concentrator-receiver system in a solar dish/Stirling power facility. Appl Therm Eng 2011;31:1780–9. doi:10.1016/j.applthermaleng.2011.02.023.

[46] Mohammad ST, Al-kayiem HH, Aurybi MA, Khlief AK. Measurement of global and direct normal solar energy radiation in Seri Iskandar and comparison with other cities of Malaysia. Case Stud Therm Eng 2020;18:100591. doi:10.1016/j.csite.2020.100591.

[47] Onubogu NO, Chong KK, Wong CW, Yew TK, Lim BH. Optical characterisation of two-stage non-imaging solar concentrator for active daylighting system. Sol Energy 2019;185:24–33. doi:10.1016/j.solener.2019.04.028.

[48] Sripadmanabhan Indira S, Vaithilingam CA, Sivasubramanian R. Performance Evaluation of a Hybrid Photovoltaic / Thermoelectric Generator System under Non-Tracking and Tracking Condition. 14th EURECA 2020 – Int. Eng. Comput. Res. Conf. "Shaping Futur. through Multidiscip. Res., vol. 335, Matec Web of Conferences; 2021. doi:https://doi.org/10.1051/matecconf/202133502009.

[49] Zhang G, Wei J, Wang Z, Xie H, Xi Y, Khalid M. Investigation into effects of non-uniform irradiance and photovoltaic temperature on performances of photovoltaic/thermal systems coupled with truncated compound parabolic concentrators. Appl Energy 2019;250:245–56. doi:10.1016/j.apenergy.2019.05.022.

[50] Kasaeian A, Daviran S, Danesh R, Rashidi A. Performance evaluation and nanofluid using capability study of a solar parabolic trough collector. Energy Convers Manag 2015;89:368–75. doi:10.1016/j.enconman.2014.09.056.